NASA TECHNICAL REPORT
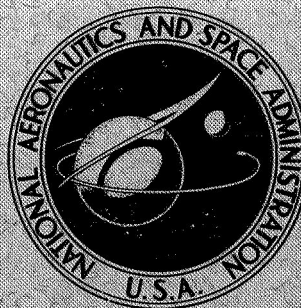
NASA TR R-433

EXPERIMENTAL DETERMINATION OF AIRPLANE MASS AND INERTIAL CHARACTERISTICS

by Chester H. Wolowicz and Roxanah B. Yancey

Flight Research Center
Edwards, Calif. 93523

NATIONAL AERONAUTICS AND SPACE ADMINISTRATION • WASHINGTON, D. C. • OCTOBER 1974

1. Report No. NASA TR R-433	2. Government Accession No.	3. Recipient's Catalog No.
4. Title and Subtitle EXPERIMENTAL DETERMINATION OF AIRPLANE MASS AND INERTIAL CHARACTERISTICS		5. Report Date October 1974
		6. Performing Organization Code
7. Author(s) Chester H. Wolowicz and Roxanah B. Yancey		8. Performing Organization Report No. H-814
9. Performing Organization Name and Address NASA Flight Research Center P. O. Box 273 Edwards, California 93523		10. Work Unit No. 501-06-05
		11. Contract or Grant No.
12. Sponsoring Agency Name and Address National Aeronautics and Space Administration Washington, D.C. 20546		13. Type of Report and Period Covered Technical Report
		14. Sponsoring Agency Code

15. Supplementary Notes

16. Abstract

This report reviews and evaluates current practices for experimentally determining airplane center of gravity, moments of inertia, and products of inertia. The techniques discussed are applicable to bodies other than airplanes.

In pitching- and rolling-moment-of-inertia investigations with the airplane mounted on and pivoted about knife edges, the nonlinear spring moments that occur at large amplitudes of oscillation can be eliminated by using the proper spring configuration.

The single-point suspension double-pendulum technique for obtaining yawing moments of inertia, products of inertia, and the inclination of the principal axis provides accurate results from yaw-mode oscillation data, provided that the sway-mode effects are minimized by proper suspension rig design. Rocking-mode effects in the data can be isolated.

The conduct of the experiments, as well as the test setup used, is a major factor in obtaining accurate results.

17. Key Words (Suggested by Author(s)) Experimental techniques Inertia determination Mass and inertia characteristics	18. Distribution Statement Unclassified – Unlimited Category: 02

19. Security Classif. (of this report) Unclassified	20. Security Classif. (of this page) Unclassified	21. No. of Pages 64	22. Price* $3.75

EXPERIMENTAL DETERMINATION OF AIRPLANE

MASS AND INERTIAL CHARACTERISTICS

Chester H. Wolowicz and Roxanah B. Yancey
Flight Research Center

INTRODUCTION

Mass and inertial characteristics—the location of the center of gravity, the moments of inertia, and the inclination of the principal axis—must be known to predict the performance and limiting flight conditions of new airplane configurations. The accuracy of such predictions is particularly important for unconventional vehicles like the lifting bodies. Furthermore, after a flight test program begins, the accuracy of the predicted mass and inertial characteristics affects the precision with which the stability and control derivatives can be determined from the flight data.

Estimates of airplane mass and inertial characteristics are made and refined during the design process. To verify the calculated characteristics, the mass distribution characteristics of a new configuration are frequently determined experimentally. However, in any experimental investigation there are limitations on the experimental setups and precautions to be observed. In these respects, the experimental techniques have continuously improved.

At first, experimental mass characteristics were determined from overhead suspensions (refs. 1 to 4). The vertical center-of-gravity position was obtained by tilting the airplane through large pitch angles and sighting the point of intersection of the line of suspension in the XZ-plane. The pitching and rolling moments of inertia were obtained by suspending the airplane as a compound pendulum. The yawing moment of inertia was obtained with the airplane suspended as a bifilar pendulum. The inclination of the principal axis was obtained from the experimentally determined ellipsoid of the inertias. However, structural, handling, and accuracy problems make it impractical to apply these methods to airplanes that weigh more than approximately 45,000 newtons.

Improved and simpler techniques were reported in reference 5. The pitching and rolling moments of inertia were obtained by the compound-pendulum method, but the airplane was supported on and pivoted about knife edges, and the restoring moments were provided by springs. The yawing moment of inertia and the inclination of the principal axis were determined by suspending the airplane support system from a vertical torsion tube in a way that permitted freedom in pitch but restrained

the airplane's rolling motion by the bending of the tube. Reference 5 is the first reported instance of finding the roll-to-yaw ratio of the response to yaw excitation as a function of pitch attitude to obtain the inclination of the principal axis. Evidently, there were practical problems that precluded further use of the torsion tube, such as difficulty in providing rigid restraint at the fixed end of the tube.

In current practices of determining mass and inertial characteristics, the vertical center-of-gravity position is obtained by tilting the airplane through a range of pitch attitudes while it is mounted on weighing scales located at jack points or the landing gear. Reference 6 considers this method to be accurate to within 5 percent. An overhead suspension method that provides more precise results is in use at the NASA Flight Research Center. To determine pitching and rolling moments of inertia, the airplane is supported on and pivoted about knife edges. To determine yawing-moment inertias and the inclination of the principal axis, a single-point suspension double-pendulum technique is used. The elementary principles of this technique are described in reference 7. Reference 8 expands on the discussion in reference 7 and provides a comprehensive theoretical treatment to insure proper rig design for the condition where the restoring-moment springs are in planes parallel to the YZ-plane. At the NASA Flight Research Center the same technique is used, but the springs are in planes parallel to the XZ-plane.

Although the literature has been concerned with improved techniques for the experimental determination of airplane mass and inertial characteristics, little mention has been made of the effects of amplitudes of oscillation on the degree of nonlinearity in the gravity-force and spring moments in pitching- and rolling-moment-of-inertia determination.

This report reviews current practices for experimentally determining the airplane center of gravity, moments of inertia, and products of inertia. The techniques discussed are applicable to bodies other than aircraft. The method used at the NASA Flight Research Center to obtain the vertical center-of-gravity position accurately is described, along with the more conventional method which involves tilting the airplane at jack points. The report provides information to facilitate the assessment of proposed experimental setups for pitching- and rolling-moment-of-inertia tests in terms of the amplitude of oscillations permissible for the accuracy desired. Finally, the NASA Flight Research Center's application of the single-point suspension double-pendulum method to determine yawing moment of inertia and product of inertia is described, and the interaction of the modes of oscillation and the requirements to suppress or minimize the undesired modes are reviewed.

SYMBOLS

Physical quantities in this report are given in the International System of Units (SI). Details concerning the use of SI are given in reference 9.

$$A = W \frac{\ell_1'}{\ell_0'}, N$$

a	length of the line of action of the spring, in yawing-moment-of-inertia tests, from the attachment point at the aircraft to the tieback stanchion (fig. 11), m

$$B = \pm \frac{\ell_2 - 2\ell_0}{\ell_{1_h}}$$

$$C_s = 4k(\ell_3')^2 (\psi \cos \delta_{sp} - \varphi_1 \sin \delta_{sp}), \text{ N-m}$$

$$D = \frac{\partial}{\partial t}$$

d	horizontal distance between the front and rear loading points used in obtaining the horizontal center-of-gravity position by the methods shown in figures 1(a), 1(b), and 2, m
d_1	horizontal distance between the center-of-gravity datum and the rear loading point used in obtaining center-of-gravity positions by the method shown in figure 2, m
E_s	ratio of the nonlinear increment in the change in spring moment to the linear change for the aircraft oscillating about a pivot
E_W	ratio of the nonlinear increment in the change in weight moment to the linear change for the inverted-pendulum concept of the aircraft oscillating about a pivot
g	acceleration due to gravity, m/sec^2
I_X, I_Y, I_Z	moments of inertia of the aircraft about the X-, Y-, and Z-body axes, respectively, kg-m^2
$(I_Y)_{cg}$	moment of inertia of the aircraft about its Y-axis passing through its center of gravity, kg-m^2
I_{Y_0}, I_{Z_0}	moments of inertia of a test-setup component (such as cradle) about the Y- and Z-axes passing through the component's center of gravity, respectively, kg-m^2
$\left(I_{X_0} + \frac{W}{g}\ell_W^2\right)_{ec}, \left(I_{Y_0} + \frac{W}{g}\ell_W^2\right)_{ec}$	moments of inertia of a test-setup component (such as cradle) about the X- and Y-pivots of oscillation, respectively, kg-m^2
I_{XZ}	product of inertia relative to aircraft X- and Z-body axes, kg-m^2
$I_{X_s Z_s}$	product of inertia of an aircraft relative to the X- and Z-axes passing through the line of suspension, kg-m^2

$\left(I_{X_s Z_s}\right)_{ts}$ $I_{X_s Z_s}$ with test-setup components included, kg-m^2

$I_{X_0 Z_0}$ product of inertia of a test-setup component relative to the X- and Z-axes passing through the component's center of gravity, kg-m^2

$\left(I_{X_0 Z_0} + m x_s z_s\right)_{ec}$ product of inertia of a test-setup component relative to the X- and Z-axes passing through the line of suspension, kg-m^2

$\left(I_Y\right)_{am}$ change in pitching moment of inertia due to apparent additional air mass effects, kg-m^2

I_{Z_s} yawing moment of inertia of an aircraft about the line of suspension, kg-m^2

$\left(I_{Z_s}\right)_{am}$ change in yawing moment of inertia of an aircraft about the line of suspension due to apparent additional air mass effects, kg-m^2

$\left(I_{Z_s}\right)_{ts}$ yawing moment of inertia of an aircraft in the test setup about the line of suspension, kg-m^2

k linear spring constant of an individual spring, N/m

k_1, k_2, k_3, k_4 spring constants of springs used in single-point suspension test setup (fig. 17), N/m

k_t torsional spring constant, N-m/rad

$k_y = \dfrac{W}{\ell_0}$, N/m

$k_\varphi = W \dfrac{\ell_1'}{\ell_0'}\left(\ell_1' + \ell_0'\right) + k_t \sin^2 \delta_{sp}$, N-m/rad

L_F, Y_F sinusoidal forcing rolling-moment input, N-m, and side force input, N, respectively

L_s, N_s, Y_s spring rolling moment, N-m, yawing moment, N-m, and side force, N, respectively

$\ell_{a/c}, \ell_W$ distance from the center of gravity of airplane and component weight, respectively, to the pivot of oscillation normal to pivot axis, m

ℓ_b length of suspension beam (used in appendix B), m

ℓ_r distance between reference rivets, defining reference longitudinal body axis (fig. 3), m

ℓ_0, ℓ_1, ℓ_2 dimensions used in pitch and roll configurations, defined in table 1 and figure 6, m

$\ell_{1_h} = \ell_1 \cos \delta_1$, m

$\ell_0', \ell_1', \ell_2', \ell_3'$ dimensions used in single-point suspension method for determining I_Z, I_{XZ}, and ε, defined in figures 11(a) and 13, m

ΔM_s change in spring moment, N-m

ΔM_W change in weight moment due to perturbation of inverted pendulum action of weight, N-m

$\left(\Delta M_W \right)_{\delta_W = 0}$ ΔM_W when pendulum arm is horizontal, N-m

$m = \dfrac{W}{g}$, kg

$m_{a/c} = \dfrac{W_{a/c}}{g}$, kg

$m_b = \dfrac{W_b}{g}$, kg

P period of oscillation, sec

P_n1, P_n2, P_n3 spring configurations in pitch tests with springs normal to moment arm extending from spring attachment point on airplane to pivot of oscillation (fig. 6)

P_v1, P_v2 spring configurations in pitch tests with springs vertical

$p, \dot{p}$ roll rate, rad/sec, and roll acceleration, rad/sec^2, respectively

$|p|, |r|$ amplitude of roll rate and yaw rate, respectively, rad/sec

$\left(\Delta |p| \right)_{RM}$ amplitude of rocking-mode roll rate in total roll response to yaw-mode excitation (fig. 15(b)), rad/sec

$\dfrac{|p|}{|r|}_\psi$ yaw-mode amplitude ratio of roll-to-yaw rate

$p_1 = \left(\dfrac{k_t}{I_{XZ}} \cos \delta_{sp} \sin \delta_{sp} \right)^{\frac{1}{2}}$

R_M, R_N vertical reaction loads on main landing wheels and nose-wheel, respectively, in center-of-gravity determination (figs. 1(a) and 1(b)), N

$R_n 1$ spring configuration in roll tests with springs normal to moment arm extending from spring attachment point on airplane to pivot of oscillation (fig. 6(c))

$r, \dot{r}$ yaw rate, rad/sec, and yaw acceleration, rad/sec^2, respectively

t time, sec

W weight, N

$\left(W \ell_W \sin \delta_W \right)_{ec}$ gravity-force moment of experimental component, N-m

$W_{a/c}$ weight of the aircraft with test-setup components removed, N

$\left(W_{a/c} \right)_{ts}$ weight of the aircraft with the weight of the test-setup components included, N

W_b weight of suspension beam (fig. 3), N

W_{bal} weight of ballast (fig. 3), N

W_{or} weight of outrigger (fig. 3), N

w loading weight in the determination of the vertical center-of-gravity position using the single-point suspension method, N

X, Y, Z axes of the airplane through its center of gravity (fig. 17)

X', Z' longitudinal and vertical reference axes, respectively, through the suspension bolt (fig. 3)

X_p longitudinal principal axis of the airplane

X_s, Y_s, Z_s axes of the airplane (with test-setup components included) passing through the center of gravity located on the line of suspension (fig. 17)

x'_b, z'_b horizontal and vertical distances, respectively, of the center of gravity of the suspension beam relative to the $X'Z'$-axes (fig. 3), m

x'_{bal}, z'_{bal} horizontal and vertical distances, respectively, of the center of gravity of the leveling ballast relative to the $X'Z'$-axes (fig. 3), m

x'_{or}, z'_{or} horizontal and vertical distances, respectively, of the center of gravity of the spring attachment outrigger relative to the $X'Z'$-axes (fig. 3), m

x'_{ref} horizontal distance from line of suspension to the body reference station (fig. 3), m

x_s, y_s, z_s horizontal, lateral, and vertical distances, respectively, of the center of gravity of an experimental component from the $X_s Y_s Z_s$-axes, m

x'_w, z'_w horizontal and vertical distances, respectively, of the loading weight, w, relative to the $X'Z'$-axes (figs. 1(c) and 3), m

$\bar{x}, \bar{z}$ distances parallel and normal, respectively, to the center of gravity of the aircraft from the datum used in ground-based determinations of the center of gravity (fig. 1(b)), m

$\Delta\bar{x}, \Delta\bar{z}$ shift in $\bar{x}$ and $\bar{z}$, respectively, due to the removal of test-setup components, m

y lateral displacement, m

$y_{st} = \dfrac{Y_F \ell'_0}{W}$, m

$\dfrac{|y|}{|y_{st}|}$ sway-mode amplification factor

$\left| -y \right|_y$ amplitude of oscillatory lateral displacement due to sway mode, m

$\bar{z}'$ vertical location of the center of gravity of the aircraft relative to the X'-axis (fig. 1(c)), m

z'_r vertical distance from the suspension bolt to the horizontal reference body axis defined by the reference rivets (fig. 3), m

$\bar{z}_r$ vertical location of the center of gravity of the aircraft to the horizontal reference body axis defined by the reference rivets, m

$\bar{z}'_{ts}$ $\bar{z}'$ value of aircraft with test-setup components included, m

δ_1 — inclination angle, relative to the horizontal, of the line from the point of attachment of the spring at the aircraft test set-up to the pivot of oscillation (in pitch and roll tests), rad

$\Delta\delta_1$ — change in δ_1 due to oscillatory perturbations, rad

$\left|\Delta\delta_1\right|$ — amplitude of $\Delta\delta_1$, rad

$\Delta\ddot{\delta}_1$ — acceleration of $\Delta\delta_1$, rad/sec^2

δ_{sp} — inclination angle of spring plane (fig. 11), rad

δ_W — inclination angle of inverted-pendulum arm of component weight, W (fig. 4), rad

$\Delta\delta_W$ — change in δ_W due to oscillatory perturbations, rad

ε — inclination of principal X-axis relative to aircraft X-axis (fig. 11), rad

θ — pitch attitude, rad

φ — roll angle, rad

$\varphi_{st} = L_F/k_\varphi$, rad

φ_0, φ_1 — roll angles of arms of double-pendulum concept of the single-point suspension (fig. 13), rad

$\left|\varphi_1\right|_y, \left|\psi\right|_y$ — amplitudes of sway-mode roll and yaw motions, respectively, rad

$\left|\varphi_1\right|_\varphi, \left|\psi\right|_\varphi$ — amplitudes of rocking-mode roll and yaw motions, respectively, rad

$\dfrac{\left|\varphi_1\right|}{\left|-y\right|_y}, \dfrac{\left|\psi\right|}{\left|-y\right|_y}$ — sway-mode amplitude ratios of roll and yaw motions of the aircraft, respectively, relative to lateral motion

$$\frac{\left|\varphi_1\right|}{\left|-y_{st}\right|} = \frac{\left|\varphi\right|}{\left|-y\right|_y}\frac{\left|y\right|}{\left|y_{st}\right|}$$

$\dfrac{\left|\varphi_1\right|}{\left|\psi\right|_\varphi}, \dfrac{\left|\varphi_1\right|}{\left|\psi\right|_\psi}$ — roll-to-yaw amplitude ratios of the aircraft for roll-mode and yaw-mode transient responses, respectively

ψ — yaw angle, rad

8

ω	frequency of oscillation, rad/sec
ω_0	frequency of oscillation of an uncoupled mode of oscillation, rad/sec
$\omega_y, \omega_\varphi, \omega_\psi$	frequency of oscillation of sway-mode, roll-mode, and yaw-mode transient responses, respectively, rad/sec
$(\omega_y)_0, (\omega_\varphi)_0, (\omega_\psi)_0$	frequency of oscillation of simple, uncoupled sway-mode, roll-mode, and yaw-mode transient responses, respectively, rad/sec

$\Delta\omega^2 = \omega^2 - \omega_0^2$, rad/sec

$\Delta(\omega_\psi)^2 = (\omega_\psi)^2 - (\omega_\psi)_0^2$, rad/sec

Subscript:

ec   experimental component

CENTER OF GRAVITY

The horizontal position of the center of gravity of an airplane can be readily determined at the time the airplane is weighed. The vertical position can be determined in several ways. The most commonly used techniques are discussed in this section and shown in figures 1(a) to 1(c).

Use of Ground-Based Loading Equipment To Determine Horizontal and Vertical Position of the Center of Gravity

The weight of an airplane and the horizontal position of the center of gravity can be obtained by placing the airplane on loading cells or platform scales with the reference X-axis horizontal and measuring the reaction forces on the two main landing wheels, R_M, and the nosewheel, R_N, and the horizontal distance from the center of the main wheel bearings to the center of the nosewheel bearing, d (fig. 1(a)). Thus

$$W = R_N + R_M \tag{1}$$

and the distance from the main wheel bearings to the center of gravity, $\bar{x}$, is obtained from

$$\bar{x} = \frac{R_N d}{W} \tag{2}$$

The precision of the results depends on the minimum count resolution of the scales,

the accuracy of the measurement of d, and the precision with which the position of the main wheel bearings is known with respect to the body station.
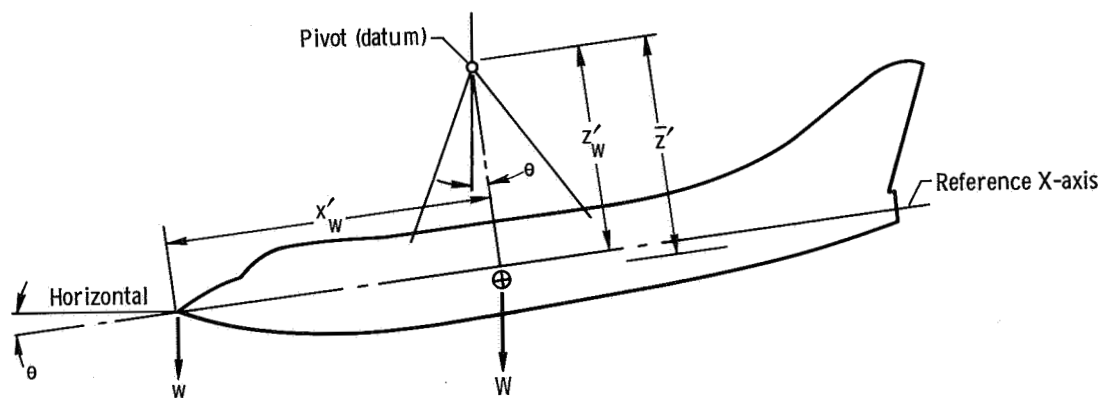
The vertical position of the center of gravity relative to a reference datum, as well as the horizontal position and the airplane weight, can be obtained by arranging the setup shown in figure 1(a) so that it allows the airplane to be tilted in the pitch
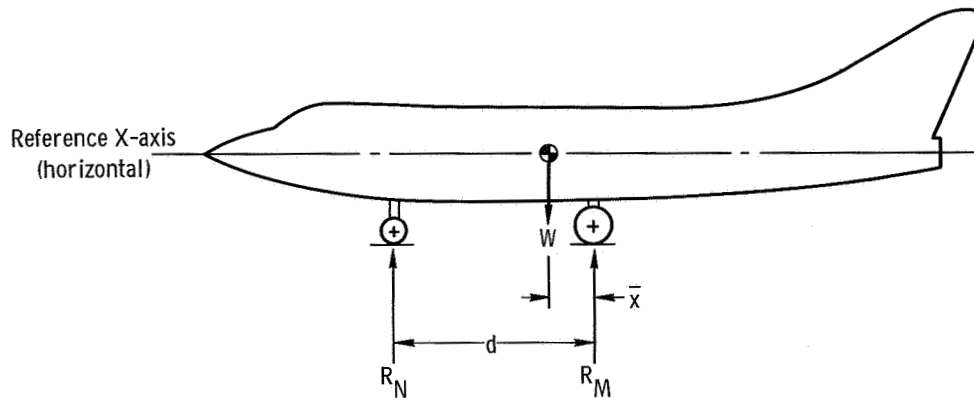
(a) Weight and horizontal position of center of gravity.
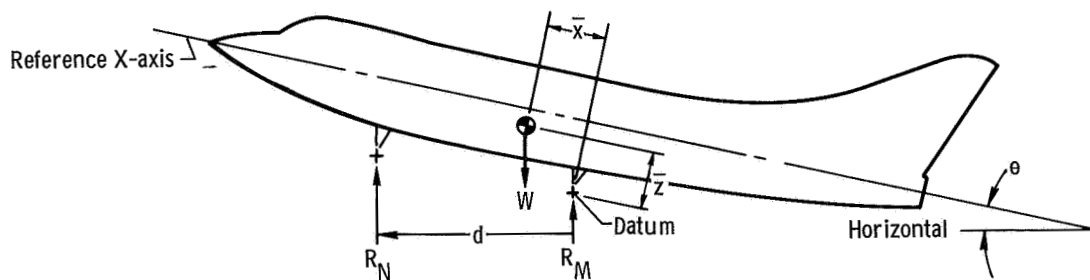
(b) Weight and vertical and horizontal position of center of gravity.

(c) Vertical position of center of gravity.

Figure 1. Experimental techniques for determining weight and center-of-gravity positions.

10

plane and then measuring the tilt angle (fig. 1(b)). The reaction forces on the scales, R_M and R_N, and the horizontal distance, d, vary as the airplane is tilted. The tilt angle is obtained by means of an inclinometer or a transit.

As shown in figure 1(b), the center of the main wheel bearings is the datum point and a datum line is extended from the datum point normal to the reference X-axis of the airplane. Thus
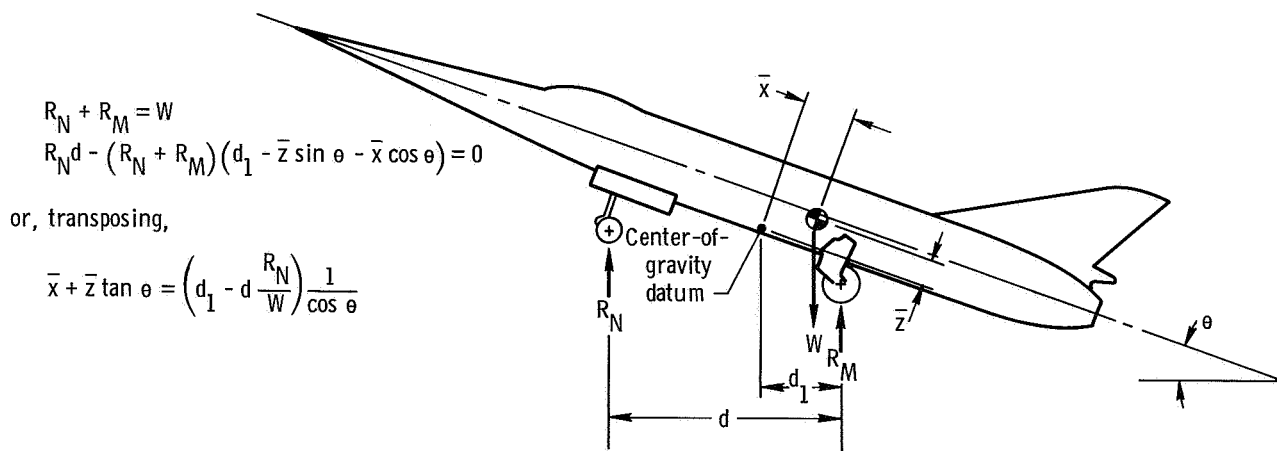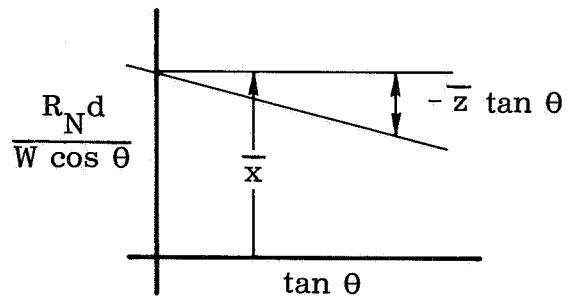
$$R_N d = W\left(\overline{x} \cos \theta - \overline{z} \sin \theta\right) \qquad (3)$$

where $\overline{x}$ is the distance parallel to the reference X-axis from the datum line to the center of gravity, and $\overline{z}$ is the distance parallel to the datum line from the datum point to the center of gravity. Then from equation (3),

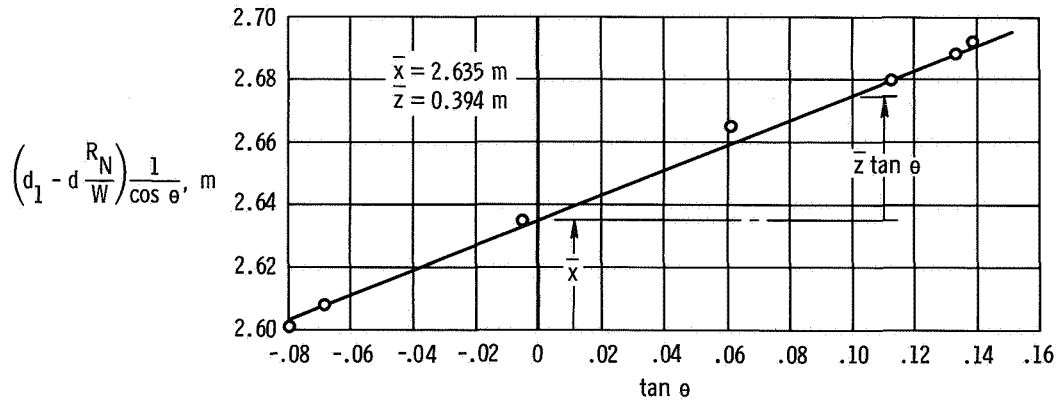$$\overline{x} - \overline{z} \tan \theta = \frac{R_N d}{W \cos \theta} \qquad (4)$$

A graphical solution for $\overline{x}$ and $\overline{z}$ in equation (4), using several inclination angles, is obtained as shown in the adjacent sketch.

Figures 2(a) and 2(b) show the experimental setup, equations, and results of a test in which the weight and vertical and horizontal positions of the center of gravity were determined for the Fairey Delta 2 airplane without fuel (ref. 10). In this experiment, a point on the body was selected as the datum point.

$$R_N + R_M = W$$

$$R_N d - \left(R_N + R_M\right)\left(d_1 - \overline{z} \sin \theta - \overline{x} \cos \theta\right) = 0$$

or, transposing,

$$\overline{x} + \overline{z} \tan \theta = \left(d_1 - d\,\frac{R_N}{W}\right)\frac{1}{\cos \theta}$$

(a) Test setup.

Figure 2. Example of the experimental determination of the horizontal and vertical position of the center of gravity of the Fairey Delta 2 airplane by tilting the airplane on weighing scales. Data are from reference 10.

The graph shows a plot with y-axis labeled $\left(d_1 - d\dfrac{R_N}{W}\right)\dfrac{1}{\cos\theta}$, m ranging from 2.60 to 2.70, and x-axis labeled $\tan\theta$ ranging from -.08 to .16. Annotations: $\bar{x} = 2.635$ m, $\bar{z} = 0.394$ m, $\bar{z}\tan\theta$, $\bar{x}$.

(b)   Horizontal and vertical position of center of gravity.

Figure 2.   Concluded.

When using this technique, precautions must be taken to insure the rigidity of the support points relative to the body and the precision of the measurement of the distances and attitude angles. Otherwise, the results may be unreliable. If flexure at the loading points cannot be eliminated, other means are necessary to determine the center of gravity.

Use of Single-Point Suspension To Determine the Vertical Position of the Center of Gravity

The vertical position of the center of gravity, as well as a refinement of the horizontal position, can be determined as byproducts of the use of a single-point suspension double-pendulum rig to obtain the inclination of the principal axis and the moment of inertia about the Z-axis. In this technique, the reference X- and Y-axes of the suspended airplane (fig. 1(c)) are leveled by the addition of ballast (normally lead shot). While the airplane is being leveled, which is usually done with a clinometer, care must be taken not to cause pitch attitude changes due to the load induced by the clinometer operator. After the airplane is level, a weight box of known weight is suspended from the front of the airplane with the point of suspension known accurately both horizontally and vertically with regard to the pivot of suspension. Known weights are added to the weight box, and the stabilized vehicle's attitude for each weight loading is measured. For each weight loading (which includes the weight box) and corresponding pitch attitude, the vertical position of the center of gravity relative to the pivot, without the weight loading, is determined as follows:

$$\bar{z}' = \frac{w\left(x'_w \cos\theta - z'_w \sin\theta\right)}{W\sin\theta}$$

$$= \frac{w}{W}\left(\frac{x'_w}{\tan\theta} - z'_w\right) \tag{5}$$

where w is the weight loading, and W is the suspended aircraft weight with experimental gear but without loading.

To insure consistent results with this technique, the following precautions should be observed:

(1) The pivot point should be as free from friction as possible.
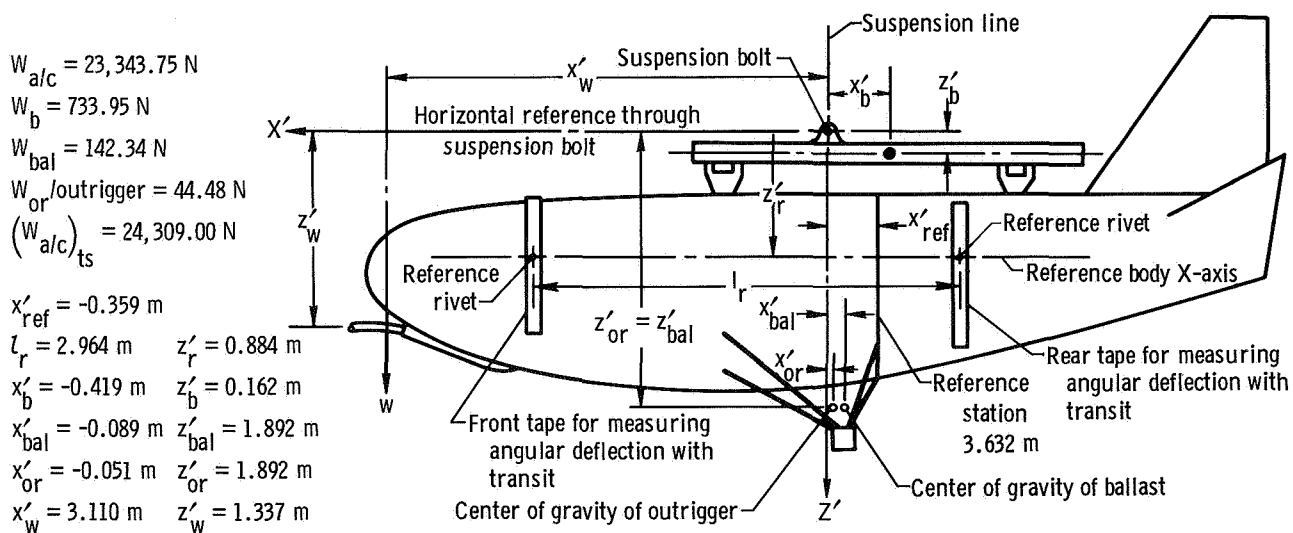
(2) The vertical distance from the pivot to the suspension point of the weight box should be as short as practical in relation to the horizontal distance to insure the maximum tilt angle for each weight condition.

(3) The sling lines of the suspension should converge and be fastened to a collecting fixture, which itself contains the eye for attachment to the suspension hook.

(4) The measurement of the tilt angle for each loading should be as accurate as possible. Good results have been obtained by using a transit to sight the vehicle's attitude by reading two rigid tape measures attached at reference points along and normal to the reference X-axis. The tapes are read at each stabilized tilt position, and the difference in the readings divided by the distance between them (measured along the X-axis) provides the tangent of the tilt angle. Using an inclinometer to measure the tilt angle has not been satisfactory.

(5) To minimize the effects of hysteresis, the loadings should be removed in reverse order of increasing load application, and the average reading for each tape at each load condition should be obtained.

Figure 3(a) shows the suspended setup used at the NASA Flight Research Center with the HL-10 lifting body vehicle. Figure 3(b) shows the vertical position of

$W_{a/c} = 23{,}343.75$ N

$W_b = 733.95$ N

$W_{bal} = 142.34$ N

$W_{or}/\text{outrigger} = 44.48$ N

$\left(W_{a/c}\right)_{ts} = 24{,}309.00$ N

$x'_{ref} = -0.359$ m

$l_r = 2.964$ m $z'_r = 0.884$ m

$x'_b = -0.419$ m $z'_b = 0.162$ m

$x'_{bal} = -0.089$ m $z'_{bal} = 1.892$ m

$x'_{or} = -0.051$ m $z'_{or} = 1.892$ m

$x'_w = 3.110$ m $z'_w = 1.337$ m

(a) Test setup.

Figure 3. Experimental setup and results obtained for the vertical position of the center of gravity of the HL-10 lifting body vehicle by using the single-point suspension method.
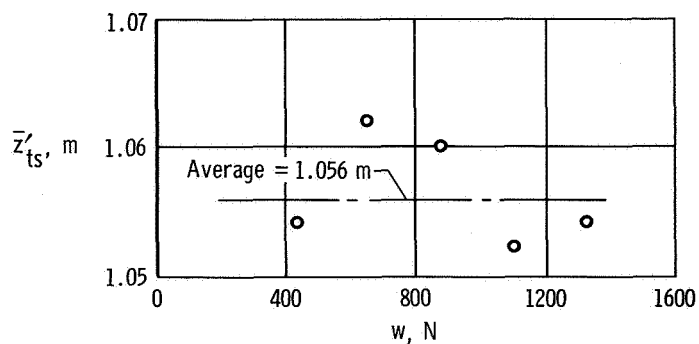
(b) *Vertical position of the center of gravity with experimental gear included.*

Figure 3. Concluded.

the center of gravity of the vehicle when weighted with the leveling ballast and the experimental gear as determined for each tilt loading, as well as the average value from all loadings. The average value is within ±0.005 meter of the spread of the test results. Appendix A summarizes the data, calculations, and results of determining the vertical and horizontal positions of the center of gravity of the vehicle.

PITCHING AND ROLLING MOMENTS OF INERTIA

The determination of pitching and rolling moments of inertia with the airplane pivoted on knife edges involves perturbations of the gravity-force moments (weight moments), restoring spring moments, and corrections for the apparent additional mass effect of the ambient air mass set in motion by the motions of the airplane. Formulas for the correction of apparent additional mass effects on the test results are given in reference 11.

If the nonlinear effects of perturbed gravity-force moments and spring moments have been minimized to the point of insignificance, the equations of motion for a knife-edge setup of a compound pendulum for the determination of pitching-moment inertia are as follows:

$$\left[I_{Y_{cg}} + \frac{W_{a/c}}{g}\ell^2_{a/c} + \sum\left(I_{Y_0} + \frac{W}{g}\ell^2_W\right)_{ec} + (I_Y)_{am}\right]\Delta\ddot{\delta}_1 = -k_t\Delta\delta_1 + \sum\left(W\ell_W \sin\delta_W\right)_{ec}\Delta\delta_1 \tag{6}$$

Letting

$$\Delta\delta_1 = \left|\Delta\delta_1\right| \sin\omega_0 t$$

where ω_0 is the natural frequency of the oscillatory response for the setup, and

14

transposing equation (6) results in the expression

$$I_Y = \frac{k_t - \sum\left(W\ell_W \sin \delta_W\right)_{ec}}{\omega_0^2} - \frac{W_{a/c}}{g} \ell_{a/c}^2 - \sum\left(I_{Y_0} + \frac{W}{g}\ell_W^2\right)_{ec} - \left(I_Y\right)_{am} \qquad (7)$$
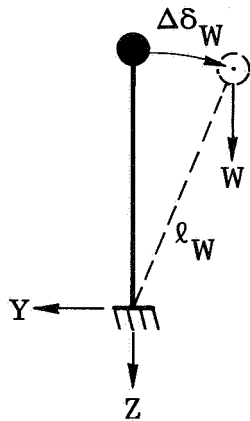
The equation for rolling moment of inertia has the same format as equation (7).

The pitching moment of inertia about the pivot axis of the experimental rig components, $\sum\left(I_{Y_0} + \frac{W}{g}\ell_W^2\right)_{ec}$, and, in the case of rolling-moment inertia, $\sum\left(I_{X_0} + \frac{W}{g}\ell_W^2\right)_{ec}$, are either calculated or, if feasible, determined experimentally. The apparent additional mass is calculated by using the formulas in reference 11.

It remains to determine the effect of the amplitude of oscillatory perturbations, $\left|\Delta\delta_1\right|$, in conjunction with the position of the airplane's center of gravity relative to the pivot and also the spring configurations, on the degree of nonlinearity in the responses to the perturbations.

<center>Gravity-Force Moments</center>

In a rolling-moment-of-inertia setup, the weight vector for the unperturbed condition normally lies in the vertical plane that extends through the pivot. During roll oscillations, the change in weight moments is accounted for by the following equation, which is for a simple inverted pendulum (see sketch) and shows the change in weight moments to be a linear function of roll displacement:

$$\Delta M_W = W\ell_W \sin \Delta\delta_W \qquad (8)$$
$$\approx W\ell_W \Delta\delta_W$$

In a pitching-moment-of-inertia setup, the weight vector for the unperturbed condition is forward or aft of the pivot and the equation takes on the following

nonlinear format:

$$\Delta M_W = W\ell_W \Delta \delta_W \left(\sin \delta_W + \frac{\Delta \delta_W}{2} \cos \delta_W \right) \qquad (9a)$$

or
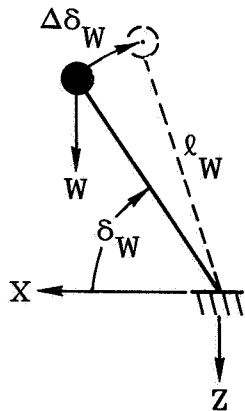
$$\Delta M_W = W\ell_W \sin \delta_W \, \Delta \delta_W \left(1 + E_W \right) \qquad (9b)$$

In equation (9b), E_W is the ratio of the nonlinear to the linear change in weight moment for the condition when the inverted pendulum is inclined at an angle, δ_W, under steady-state conditions. The ratio E_W is a function of both the magnitude and the sign of the perturbation angle, $\Delta\delta_W$, as shown in figure 4. As the figure shows, the effects of nonlinearity can be significant with increasing $\Delta\delta_W$ in one direction. However, during oscillatory motion, if $\Delta\delta_W$ has the same positive and negative amplitudes, the algebraic subtraction of equation (9a) results in the
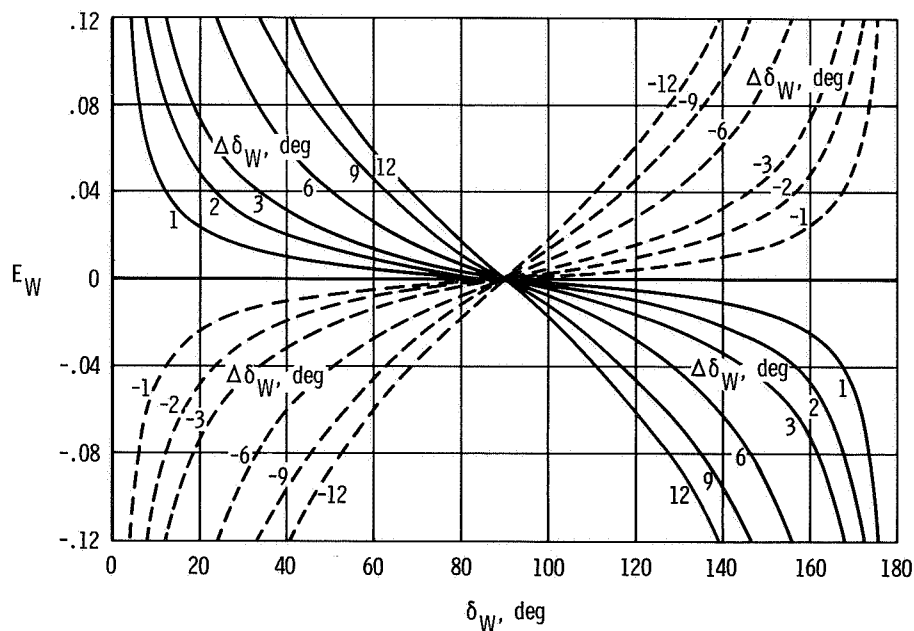
Figure 4. Ratio of nonlinear to linear increment of change in weight moment as a function of steady-state and perturbed inclinations δ_W and $\Delta\delta_W$, respectively (eq. (9b)).

16

double-amplitude expression $2\Delta M_W = 2W\ell_W \sin \delta_W |\Delta \delta_W|$. Thus, the nonlinearity would cancel out. On the other hand, the algebraic addition of equation (9a) results in a net $\Delta M_W = 2W\ell_W \sin \delta_W |E_W|$ instead of zero, indicating that there is a tendency for the zero datum of the time history of the pitching-moment perturbations to shift. It should be noted that when δ_W approaches 0°, equation (9a) reduces to the non-linear expression

$$\left(\Delta M_W\right)_{\delta_W = 0} = \frac{1}{2} W\ell_W \left(\Delta \delta_W\right)^2 \tag{10}$$

Spring Moments

A number of options are available in the layout of the springs in the pitching- and rolling-moment-of-inertia test setups. For pitch setups, the single spring (or its equivalent) in a simple spring installation may be forward or rearward of the pitch pivot. For roll setups, identical sets of springs are usually attached to the vehicle on each side of the pivot below the spring mounting points of the experimental setup to provide a stabilizing restoring couple during roll perturbations. Two sets of springs can also be used in pitch setups.

Regardless of the spring setup, the springs must be carefully calibrated and pretensioned to make sure that they operate within their linear range during perturbations. A typical calibration curve is shown in figure 5.
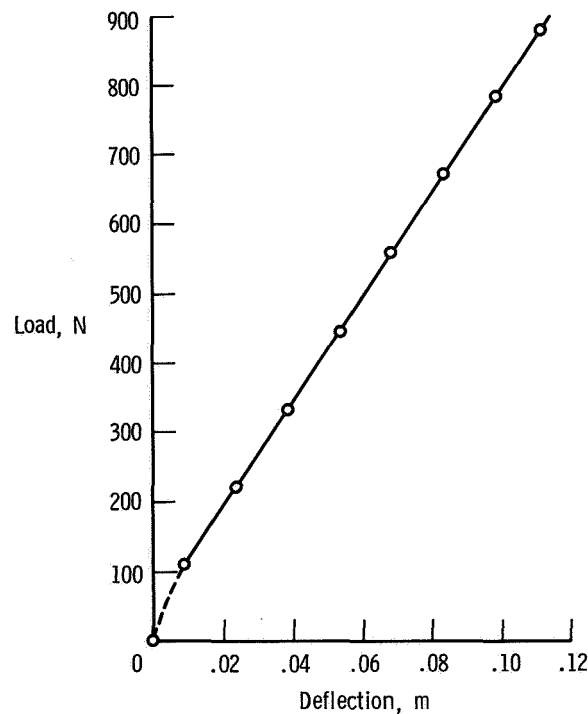

Figure 5. Typical calibration curve of a tension spring with looped ends. k = 7544 N/m.

Springs normal to the moment arm at point of spring attachment. — For single spring configurations, used in pitching-moment-of-inertia investigations, with the springs normal to the moment arm that extends from the spring attachment point to the pivot (figs. 6(a) and 6(b)), the perturbated spring moment can be represented by the following equation:

$$\Delta M_s = -k\ell_1^2 \Delta\delta_1 \left(1 + E_s\right) \tag{11}$$

where k is the linear spring constant, ℓ_1 is the length of the moment arm, and E_s is the ratio of the nonlinear increment in the change in spring moment to the linear change. For the configuration identified as $P_n 1$ in figure 6(a),

$$E_s = -\frac{\dfrac{\ell_2}{\ell_1}\left(\dfrac{\ell_2}{\ell_1} + \dfrac{3}{4}\Delta\delta_1\right)}{2\left(\dfrac{\ell_2}{\ell_1} + \Delta\delta_1\right)^2}\left(\Delta\delta_1\right)^2 \tag{12a}$$

For the configuration identified as $P_n 2$ in figure 6(b),

$$E_s = -\frac{\dfrac{\ell_2}{\ell_1}\left(\dfrac{\ell_2}{\ell_1} - \dfrac{3}{4}\Delta\delta_1\right)}{2\left(\dfrac{\ell_2}{\ell_1} - \Delta\delta_1\right)^2}\left(\Delta\delta_1\right)^2 \tag{12b}$$

Equations (12a) and (12b) and the plotted ratios in figures 6(a) and 6(b) show that the only difference in configurations $P_n 1$ and $P_n 2$ is the change in the sign of $\Delta\delta_1$. For both configurations, the direction of the perturbation, $\Delta\delta_1$, affects the magnitude, but not the sign, of E_s.

For amplitudes of $\Delta\delta_1$ of 2° or less, E_s is negligible (-0.001 or less). Even at $\Delta\delta_1 = 4°$, E_s is only approximately -0.005. However, for large amplitudes of $\Delta\delta_1$, 10° for example, the ratio is significant.
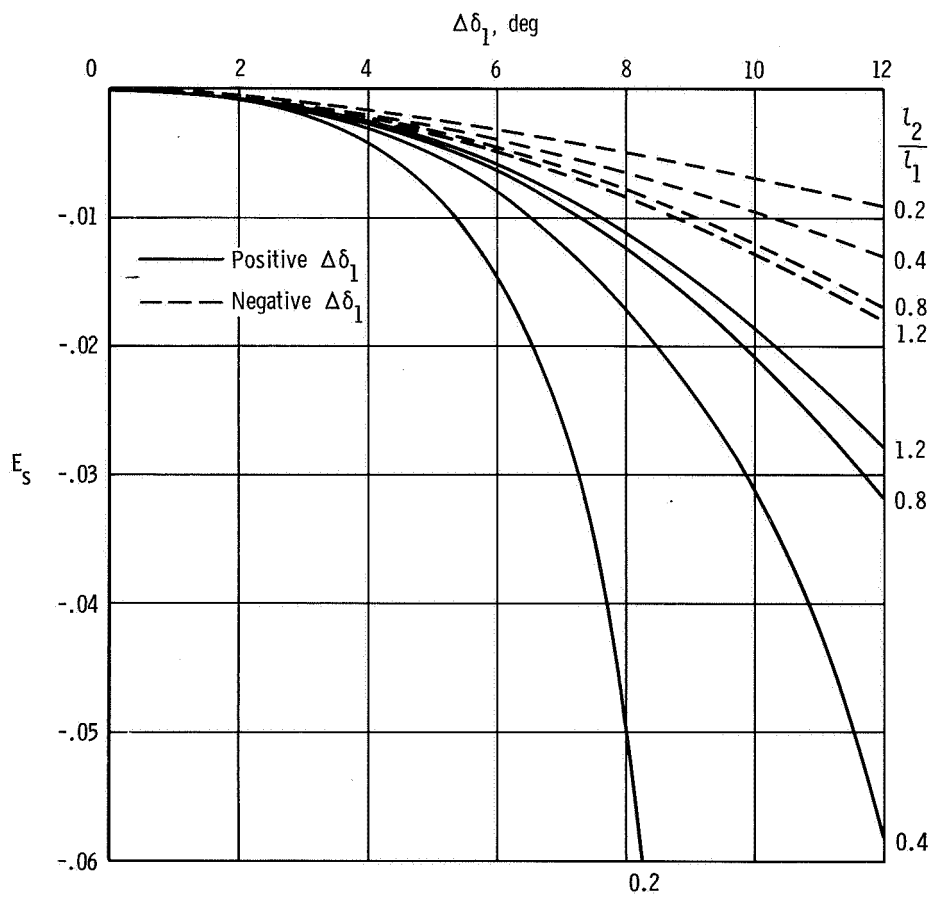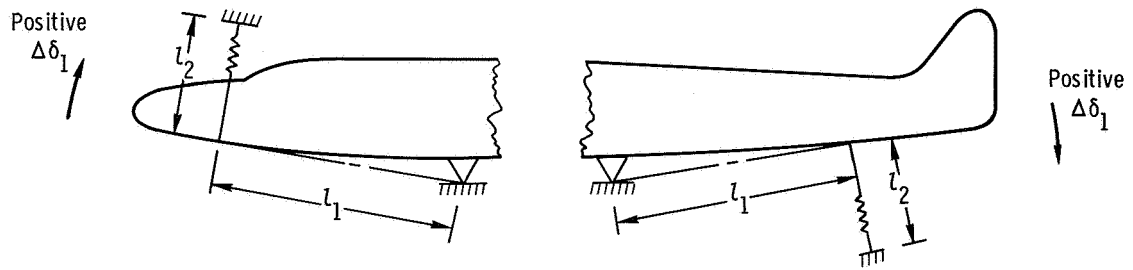
Figure 6(c) shows spring configurations for pitching- and rolling-moment-of-inertia investigations in which the configuration has identical springs on each side of the pivot and identical moment arms normal to the springs from the spring attachment points to the pivot to provide a restoring couple. In these configurations, the change in spring moment due to perturbations can be determined from the expression

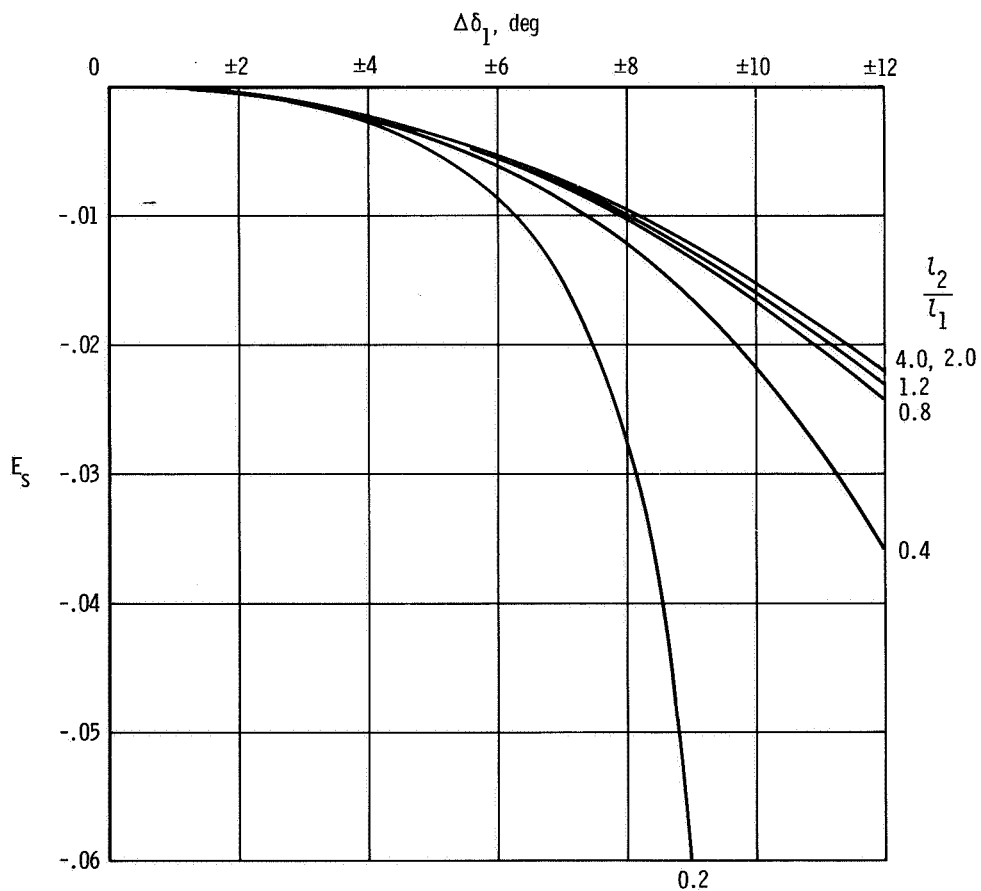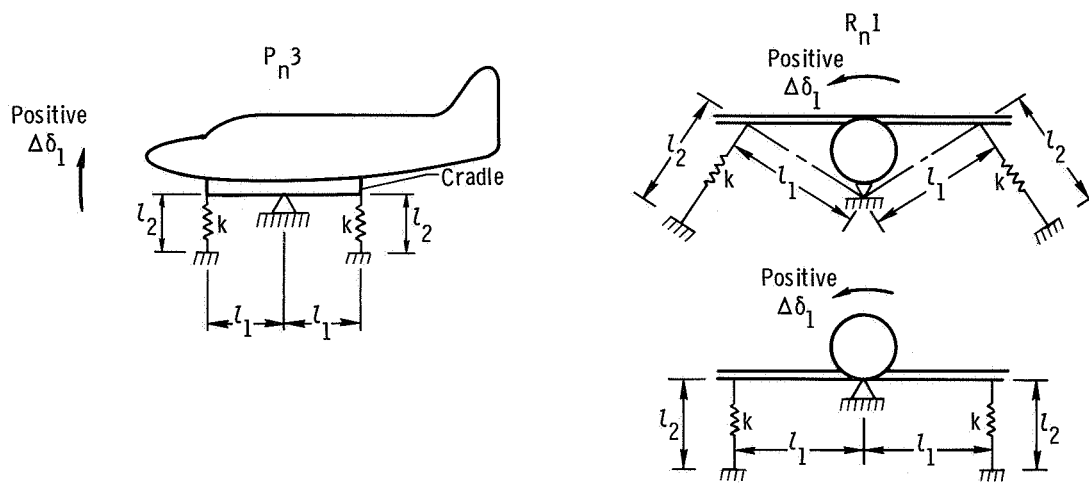$$\Delta M_s = -2k\ell_1^2 \Delta\delta_1 \left(1 + E_s\right) \tag{13}$$

18
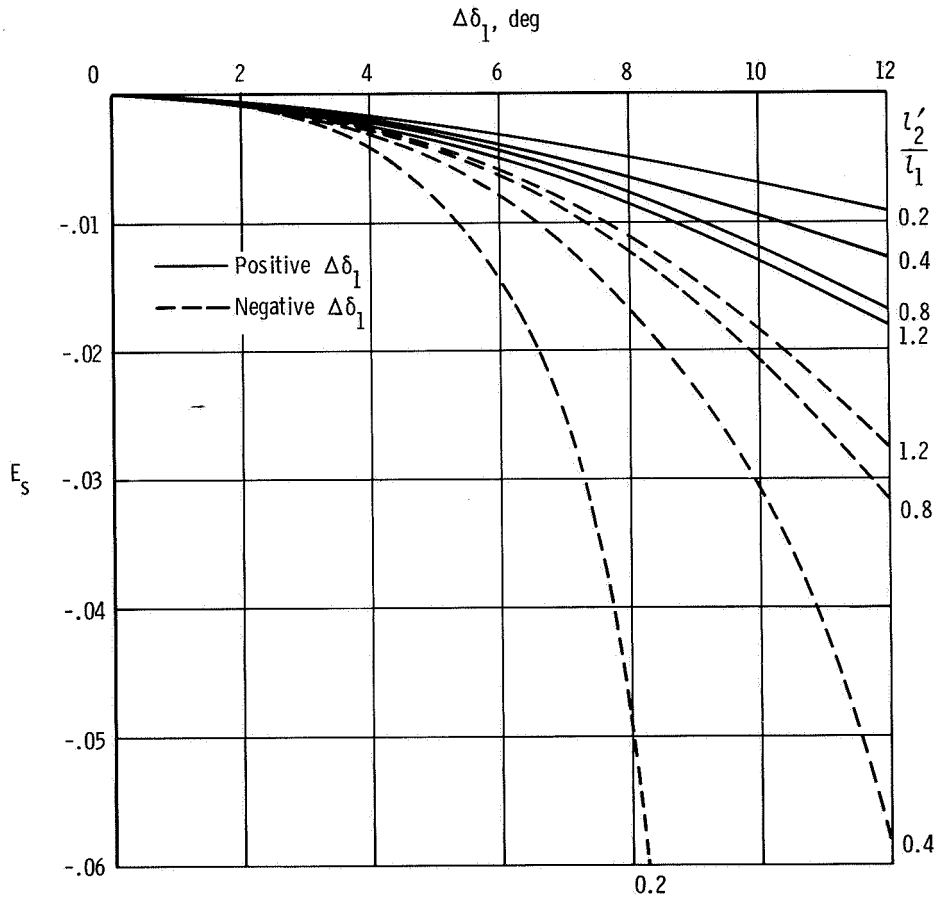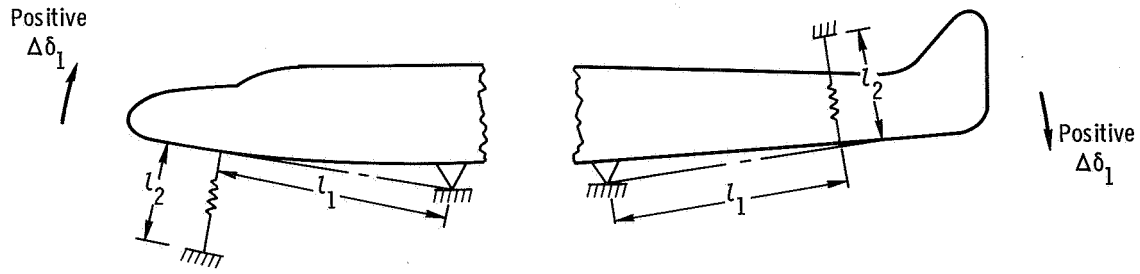
(a) Spring configuration $P_n 1$ for pitch.

Figure 6. Ratio of nonlinear to linear increment of change in spring moment as a function of $\Delta \delta_1$ and $\dfrac{l_2}{l_1}$. Spring normal to moment arm at point of attachment to airplane.

(b) Spring configuration $P_n 2$ for pitch.

Figure 6. Continued.

(c) Spring configurations P_n3 for pitch and R_n1 for roll.

Figure 6. Concluded.

where E_s is obtained from figure 6(c) or the following equation:

$$E_s = -\frac{1}{2}\left(\frac{\ell_2}{\ell_1}\right)^2 \frac{(\Delta\delta_1)^2}{\left[\left(\frac{\ell_2}{\ell_1}\right)^2 - (\Delta\delta_1)^2\right]} \left\{1 + \frac{1}{2} \frac{(\Delta\delta_1)^2}{\left[\left(\frac{\ell_2}{\ell_1}\right)^2 - (\Delta\delta_1)^2\right]}\right\} \tag{14}$$

It is apparent that E_s is a function of both $\left(\dfrac{\ell_2}{\ell_1}\right)^2$ and the magnitude, but not the sign, of $\Delta\delta_1$.

Although configurations with springs normal to the moment arm at the spring attachment point are generally considered to provide linear spring moment characteristics over a large range of perturbations, figure 6 indicates that this is not necessarily true. As shown below, the nonlinear effects are negligible over a larger perturbation range for some vertical-spring configurations.

Vertical springs.— For single vertical-spring configurations used in pitching-moment-of-inertia studies, the change in the spring moment due to perturbations is determined from the following expression in which it is desired to minimize the nonlinear error ratio, E_s^-:

$$\Delta M_s = -k\ell_{1_h}^2 \Delta\delta_1 \left(1 + E_s\right) \tag{15}$$

Two configurations, P_v1 and P_v2, of single vertical springs mounted forward of the pivot (and their mathematical equivalents with the springs rearward of the pivot) are illustrated in the following sketches, which also indicate the positive direction of the quantities shown:

P_v1 configuration

P_v2 configuration

22
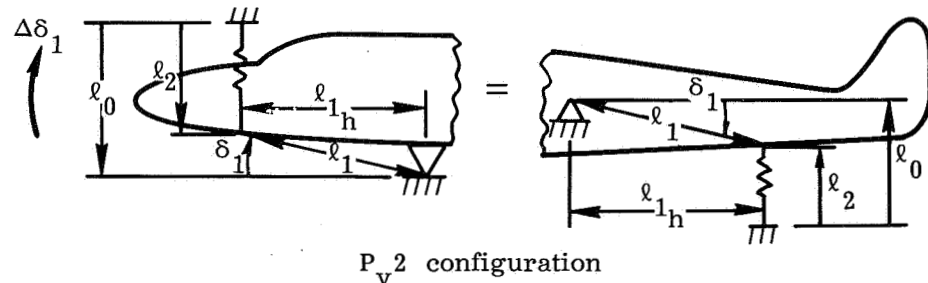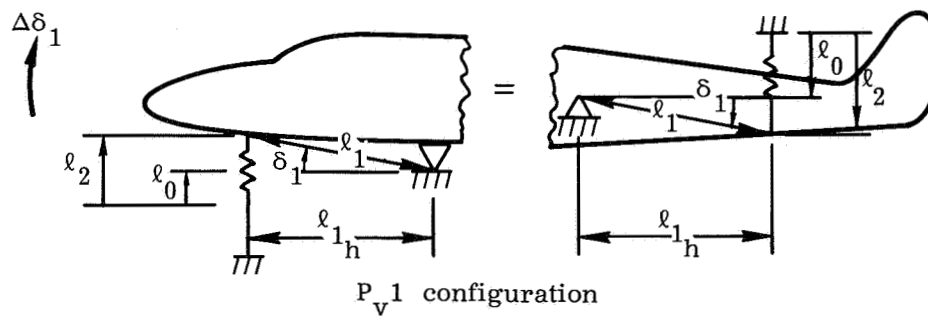
For configuration P_v1, the expression for E_s is

$$E_s = -\frac{\left\{\begin{array}{l} \dfrac{\ell_2}{\ell_{1_h}}\left[\dfrac{\ell_2}{\ell_{1_h}} + \dfrac{3}{4}(\Delta\delta_1)\right](\Delta\delta_1)^2 \\[2mm] + \left[2\left(\dfrac{\ell_2}{\ell_{1_h}}\right)^2 - (\Delta\delta_1)^2\right](\Delta\delta_1)\tan\delta_1 \\[2mm] - \left[3\left(\dfrac{\ell_2}{\ell_{1_h}}\right) + 2(\Delta\delta_1)\right](\Delta\delta_1)\tan^2\delta_1 \end{array}\right\}}{2\left(\dfrac{\ell_2}{\ell_{1_h}} + \Delta\delta_1\right)^2} \tag{16}$$

Since the P_v2 configuration is an inversion of the P_v1 configuration, changing the signs of δ_1 and $\Delta\delta_1$ in the equation for P_v1 results in the following equation for P_v2:

$$E_s = -\frac{\left\{\begin{array}{l} \dfrac{\ell_2}{\ell_{1_h}}\left[\dfrac{\ell_2}{\ell_{1_h}} - \dfrac{3}{4}(\Delta\delta_1)\right](\Delta\delta_1)^2 \\[2mm] + \left[2\left(\dfrac{\ell_2}{\ell_{1_h}}\right)^2 - (\Delta\delta_1)^2\right](\Delta\delta_1)\tan\delta_1 \\[2mm] + \left[3\left(\dfrac{\ell_2}{\ell_{1_h}}\right) - 2(\Delta\delta_1)\right](\Delta\delta_1)\tan^2\delta_1 \end{array}\right\}}{2\left(\dfrac{\ell_2}{\ell_{1_h}} - \Delta\delta_1\right)^2} \tag{17}$$

It should be noted that when $\delta_1 = 0$, the equations reduce to equations (12a) and (12b), which are for configurations in which the springs are normal to the moment arm at the spring attachment point.

The nonlinear increment ratio, E_s, is plotted in figures 7(a) to 7(h) as a function of $\tan\delta_1$ and $\Delta\delta_1$ for a series of values of $\dfrac{\ell_2}{\ell_{1_h}}$ for configuration P_v1.

The values of E_s for configuration P_v2 can be obtained from figures 7(a) to 7(h) by reversing the signs of $\tan\delta_1$ and $\Delta\delta_1$. The values of E_s in the figure for

tan $\delta_1 = 0$ are the values shown in figures 6(a) and 6(b) for the configuration in which the springs are normal to the moment arm that extends from the spring attachment point to the pivot. Figure 7 shows that for each value of $\frac{\ell_2}{\ell_{1_h}}$ there is a trend toward a crossover point, which is also a function of $\tan \delta_1$, where $E_s = 0$. These crossover points represent the optimum design conditions for the single vertical-spring configuration, and when so configured, the single vertical-spring setup is superior to the spring configurations shown in figures 6(a) and 6(b) insofar as the effects of nonlinearity are concerned.
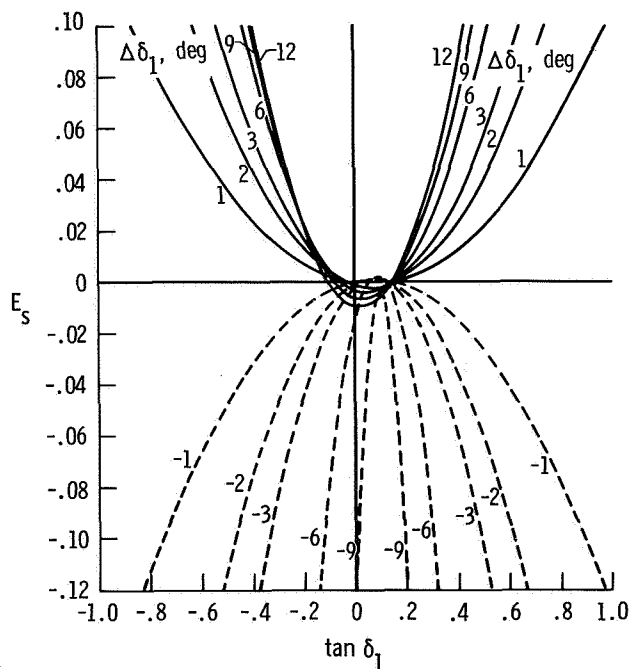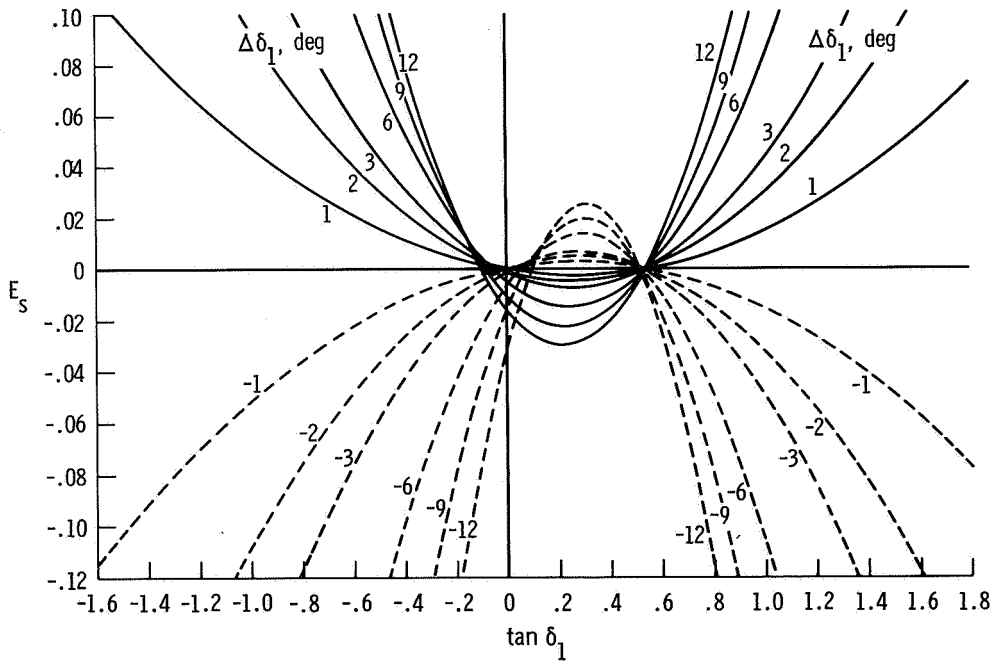

(a) $\dfrac{l_2}{l_{1_h}} = 0.2$.

Figure 7. Ratio of nonlinear to linear increment of change in single vertical-spring configuration $P_v 1$ as a function of $\tan \delta_1$, $\Delta\delta_1$, and $\dfrac{l_2}{l_{1_h}}$ for several values of $\dfrac{l_2}{l_{1_h}}$.
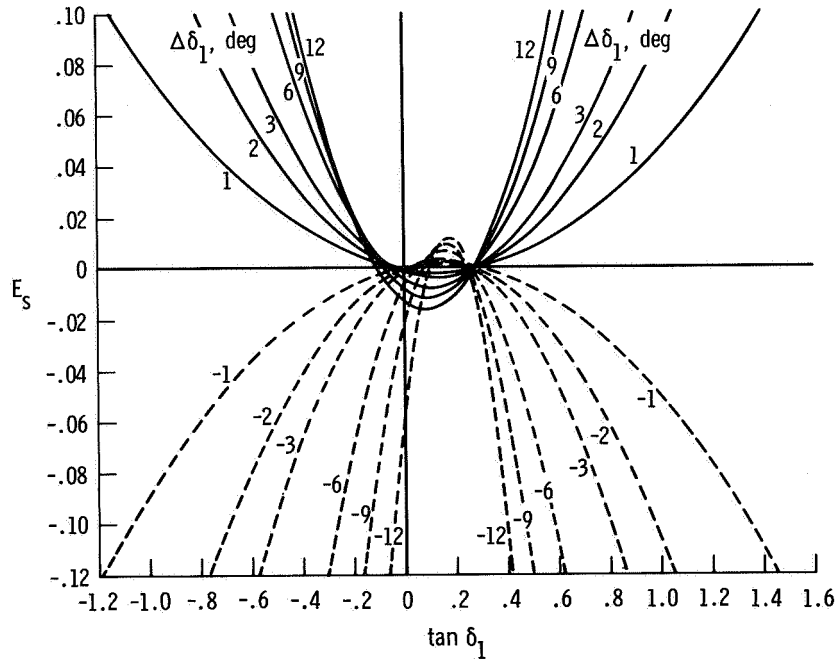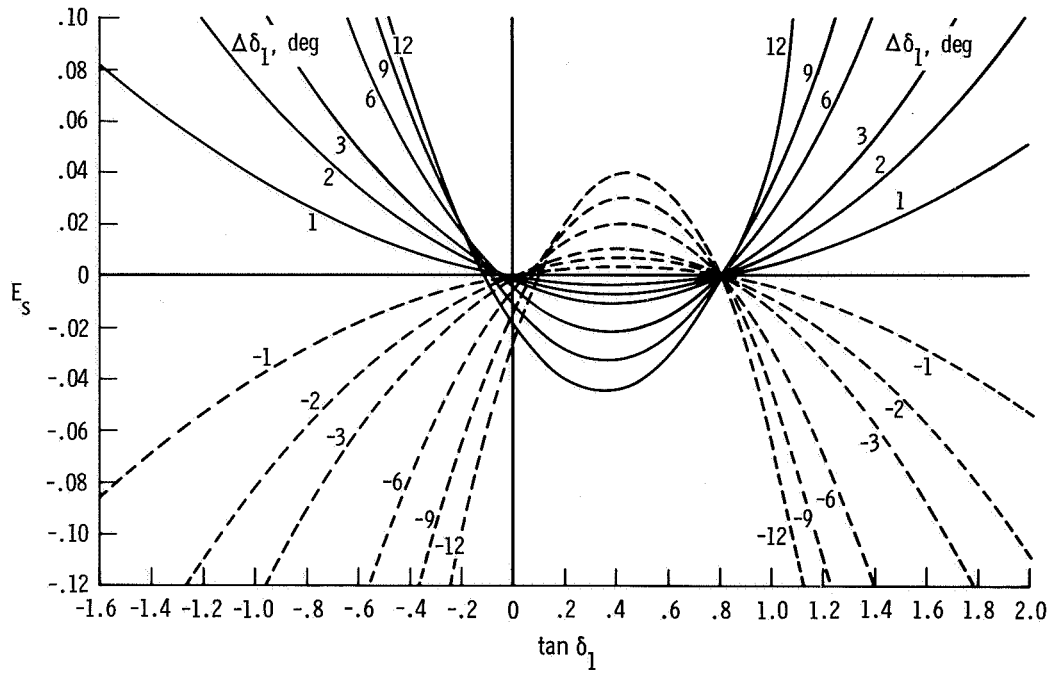
(b) $\dfrac{l_2}{l_{1_h}} = 0.4.$

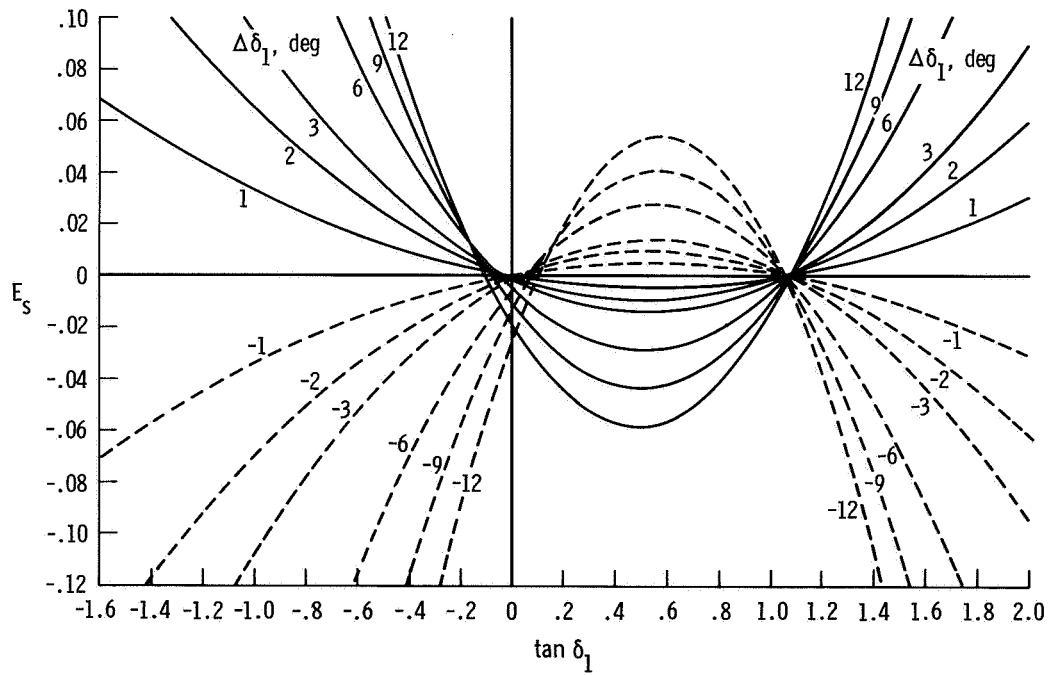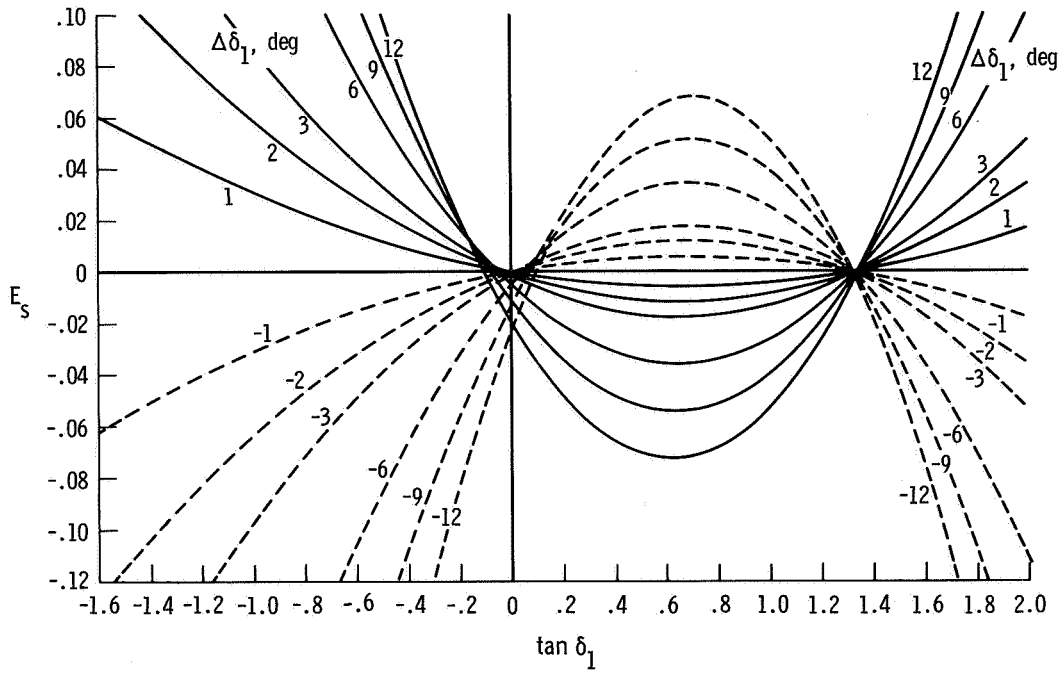

(c) $\dfrac{l_2}{l_{1_h}} = 0.8.$

Figure 7. Continued.

(d) $\dfrac{l_2}{l_{1_h}} = 1.2$.

(e) $\dfrac{l_2}{l_{1_h}} = 1.6$.

Figure 7. Continued.

(f) $\dfrac{l_2}{l_{1_h}} = 2.0.$
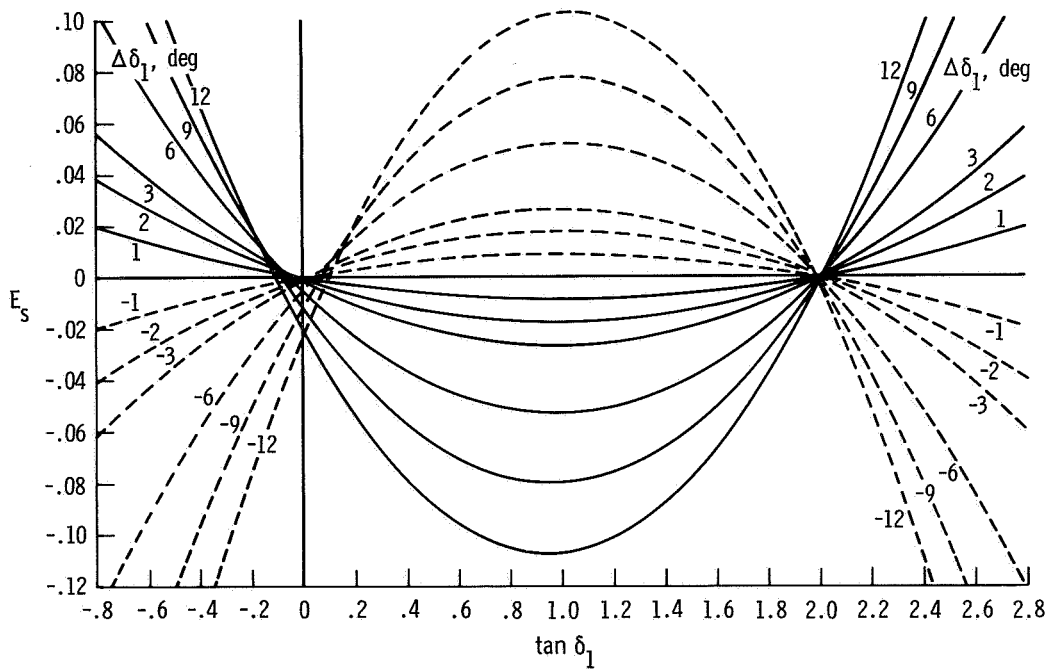
(g) $\dfrac{l_2}{l_{1_h}} = 3.0.$

Figure 7. Continued.
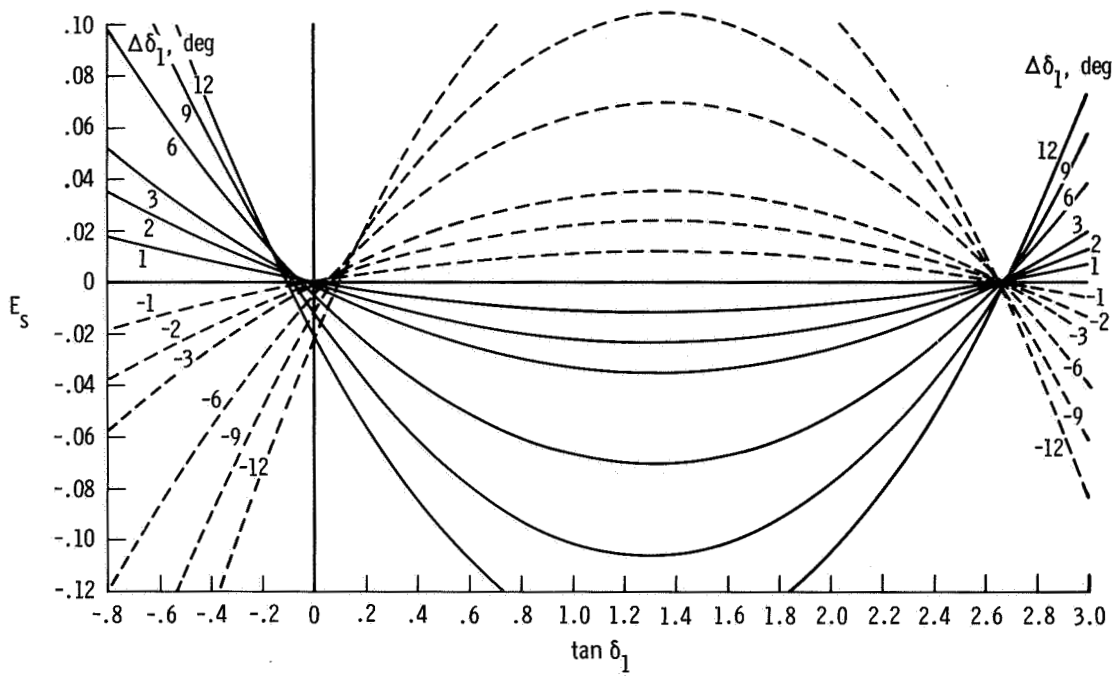
$$(h) \quad \frac{l_2}{l_{1_h}} = 4.0.$$

Figure 7. Concluded.

Figure 7 also shows that if E_s is to be held within a prescribed limit (for example, less than 0.005), the permissible magnitude of the perturbation is governed by δ_1 and $\frac{\ell_2}{\ell_{1_h}}$.

When the vertical springs are mounted symmetrically about a vertical plane of symmetry that passes through the pivot axis, as in rolling-moment-of-inertia setups, E_s in the spring moment equation

$$\Delta M_s = -2k\ell_{1_h}^2 \, \Delta\delta_1 \left(1 + E_s\right) \tag{18}$$

is defined by the expression

$$E_s = -\frac{B^2\left(\Delta\delta_1\right)^2}{2\left[\left(\frac{\ell_2}{\ell_{1_h}}\right)^2 - \left(\Delta\delta_1\right)^2\right]} \left\{ 1 + \frac{\left(\Delta\delta_1\right)^2}{2\left[\left(\frac{\ell_2}{\ell_{1_h}}\right)^2 - \left(\Delta\delta_1\right)^2\right]} \right\} \tag{19}$$

28

where, as shown in figure 8,

$$B = \pm \frac{\ell_2 - 2\ell_0}{\ell_{1_h}}$$ (20)

It is apparent from equation (19) that E_s can be eliminated by making B equal to zero. This can be accomplished by making the length ℓ_2 equal to twice the length of ℓ_0 (eq. (20)); that is, by arranging ℓ_2 so that it is bisected by the horizontal projection from the pivot.

The nomograph in figure 8 can be used to obtain values of E_s for different values of $\Delta\delta_1$ for any two-spring couple configuration. For a limited prescribed value of E_s and a fixed value of $\frac{\ell_0}{\ell_{1_h}}$, the nomograph can be used to obtain the limiting values of $\Delta\delta_1$ for different values of $\frac{\ell_2}{\ell_{1_h}}$. For a prescribed limiting value of E_s at a set value of $\frac{\ell_2}{\ell_{1_h}}$, it can be used to obtain the value of $\frac{\ell_0}{\ell_{1_h}}$ for a selected upper limit of $\Delta\delta_1$. For example, for the configuration shown in the upper left of the figure, in which the springs are below the attachment points, let $E_s \leqq 0.005$, $\frac{\ell_2}{\ell_{1_h}} = 0.6$, and $\Delta\delta_1 = \pm4.5°$. From the right side of the nomograph, find the intersection of $\Delta\delta_1 = \pm4.5$ and $\frac{\ell_2}{\ell_{1_h}} = 0.6$ and draw a horizontal line to the left. From the left side of the nomograph, draw a vertical line from $E_s = -0.005$ and note the value of B at the point where the lines intersect. In this example, $B = \pm0.8$. Now if

$$B = \frac{\ell_2}{\ell_{1_h}} - 2\frac{\ell_0}{\ell_{1_h}}$$

then

$$\pm0.8 = 0.6 - 2\frac{\ell_0}{\ell_{1_h}}$$

from which

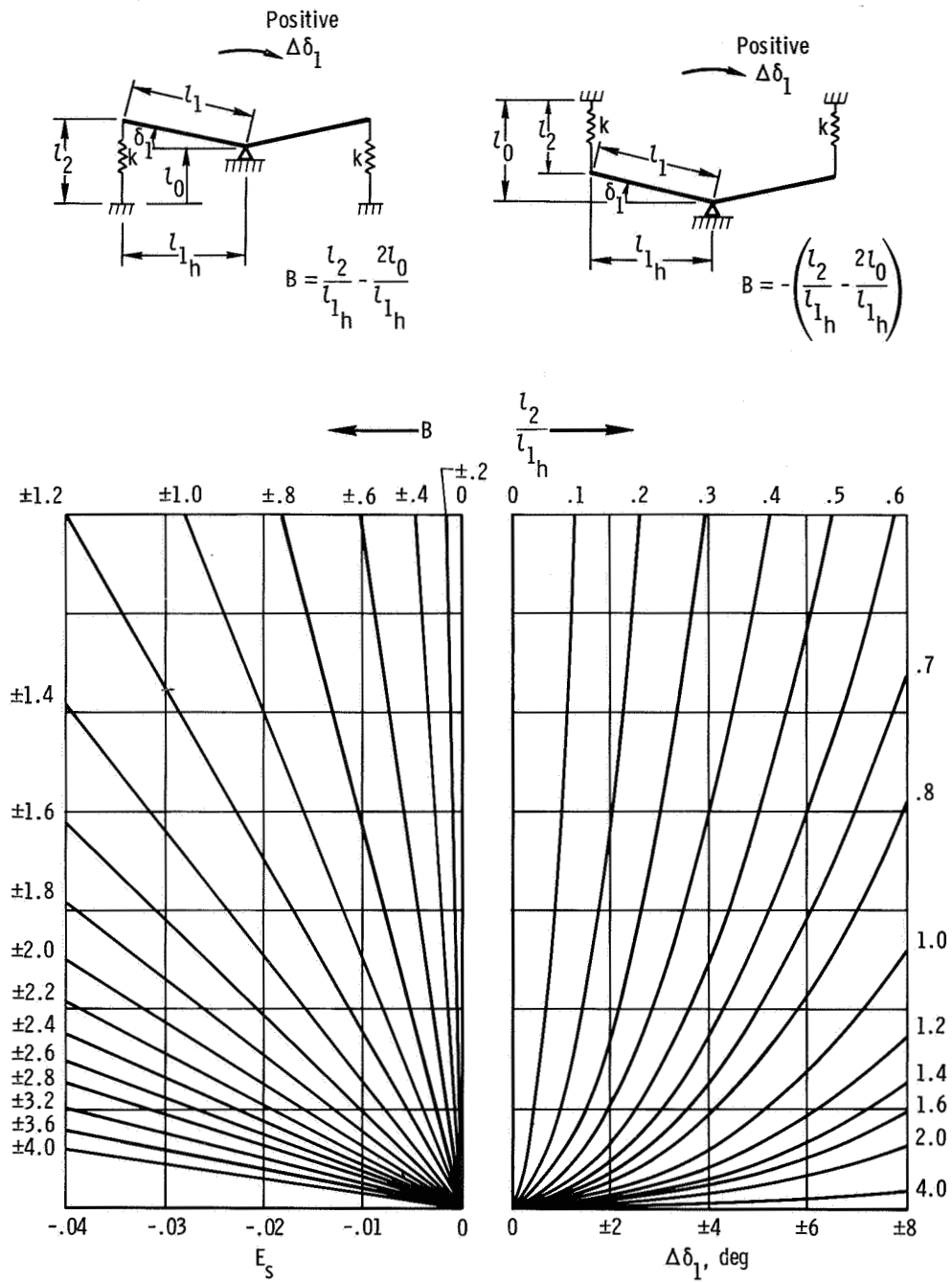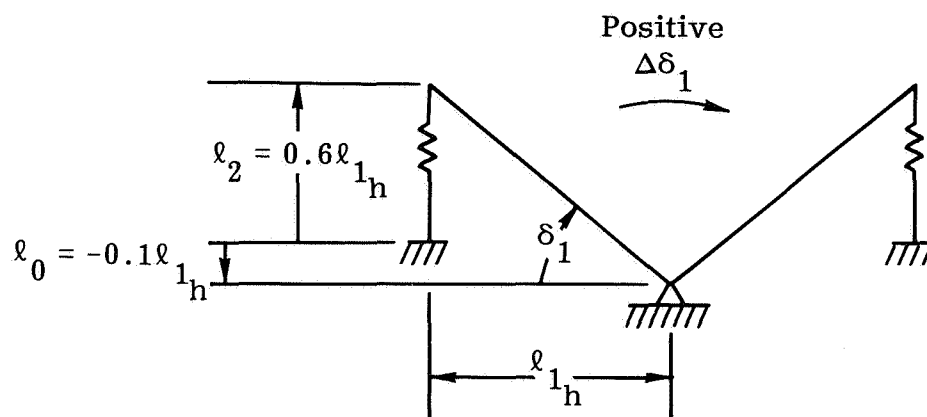$$\frac{\ell_0}{\ell_{1_h}} = -0.1 \text{ or } 0.7$$

Figure 8. Variation of nonlinear increment ratio of two vertical springs, configured to provide a restoring couple, as a function of $\Delta\delta_1$, $\dfrac{l_2}{l_{1_h}}$, and $\dfrac{l_2}{l_{1_h}} - \dfrac{2l_0}{l_{1_h}}$.

or, as shown in the following sketches,

Positive
$\Delta\delta_1$

$\ell_2 = 0.6\ell_{1_h}$

$\ell_0 = -0.1\ell_{1_h}$

δ_1

ℓ_{1_h}

or

Positive
$\Delta\delta_1$

ℓ_{1_h}

$\ell_0 = 0.7\ell_{1_h}$

$\ell_2 = 0.6\ell_{1_h}$
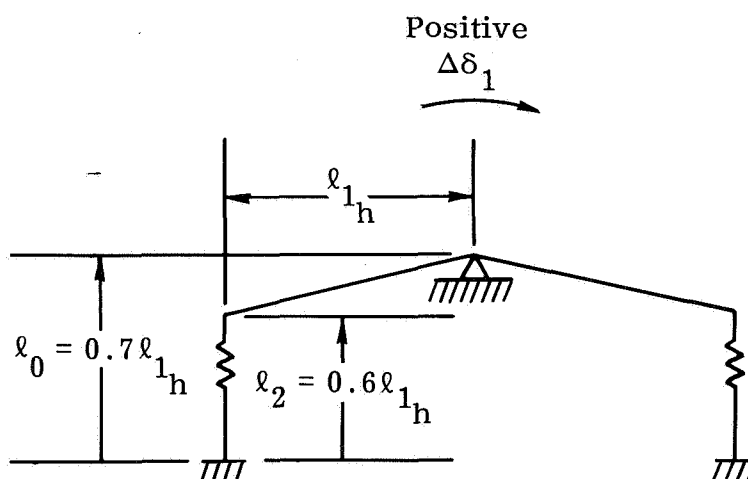
If the stipulated design conditions are applied to the configuration shown in the upper right of figure 8, in which the springs are above the attachment point, the results would be a mirror image of the preceding results.

Practical Considerations in Setting Up the Experimental Installation

Unless care is taken in every detail of an experimental setup for pitch and roll investigations, difficulties may be encountered. During one experiment to determine the pitching moment of inertia in which the aircraft was supported at the wing jack points and oscillated with the spring at the nose, the wing, which had been considered rigid, flexed as the aircraft oscillated. This flexing caused the axis of rotation to shift forward and downward from the line through the jack points.

A common error is using flexible cables to tie back the springs. Flexible cables should not be used, since they can constitute springs in series with the actual

springs, resulting in a softer spring system than intended or accounted for. Using rods for tiebacks alleviates this problem. It should also be noted that on some aircraft the rear portion of the fuselage is relatively flexible, so that attaching the spring to it alters the effective spring constant. The same problem can arise if the springs are attached to the wings. Thus, the springs should be attached to the cradle, or, if they are attached to parts of the structure that are suspected of being flexible, bracing should be set up from the cradle to the spring attachment point.

Inertia characteristics are usually determined for no-fuel conditions because the sloshing of the fuel tends to introduce a beat action into the transient oscillatory response after excitation. When inertia determination is attempted with fuel on board, the difference between the oscillatory mode of the sloshing fuel and that of the experimental setup should be as large as practical to make it possible to isolate the beat action.

Since the experimental setups for determining the pitching and rolling moments of inertia can involve substantial effects of such experimental accessories as cradles (fig. 9), the vertical and horizontal positions of the center of gravity for the clean

Figure 9. Experimental setup for determining the rolling moment of inertia.

vehicle and the experimental components must be known. The center-of-gravity positions for the clean vehicle can easily be determined experimentally by following the procedures discussed earlier. The horizontal and vertical positions of the center of gravity of the experimental accessories can be calculated and verified, at least in part, by experiment.

DETERMINING THE PRODUCT OF INERTIA AND YAWING MOMENT OF INERTIA BY THE SINGLE-POINT SUSPENSION DOUBLE-PENDULUM METHOD

Until the single-point suspension double-pendulum method described in reference 7 was introduced, the experimental determination of the product of inertia was difficult and usually unsatisfactory. In the single-point suspension double-pendulum method, which provides more accurate results, the airplane is suspended by a sling from a point at the end of a suspension line (figs. 10(a) and 10(b)). The suspension

(a) *Springs oriented crosswise.*   E-4425

Figure 10. Experimental setup for determining the yawing moment of inertia, the product of inertia, and the inclination of the principal axis using the single-point suspension method.

(b) Springs oriented lengthwise.   E-14681

Figure 10. Concluded.

line is, in effect, a torsion-free cable. The other end of the line is attached to a crane hook. The sling system itself is a rigid assembly. Yaw and roll restraint is provided by two sets of springs whose lines of action lie in a common plane (fig. 11(a)). The springs are selected and arranged to provide a spring couple vector in the XZ-plane of symmetry, which acts normal to the spring plane. One component of the vector provides restraint in yaw; the other provides restraint in roll (fig. 11(b)).

The crosswise spring configuration shown in figure 10(a) was used in the study of reference 7 and was given extensive theoretical treatment in reference 8. The longitudinal spring configuration shown in figures 10(b) and 11(a), which is the arrangement used at the NASA Flight Research Center, is considered in this report.
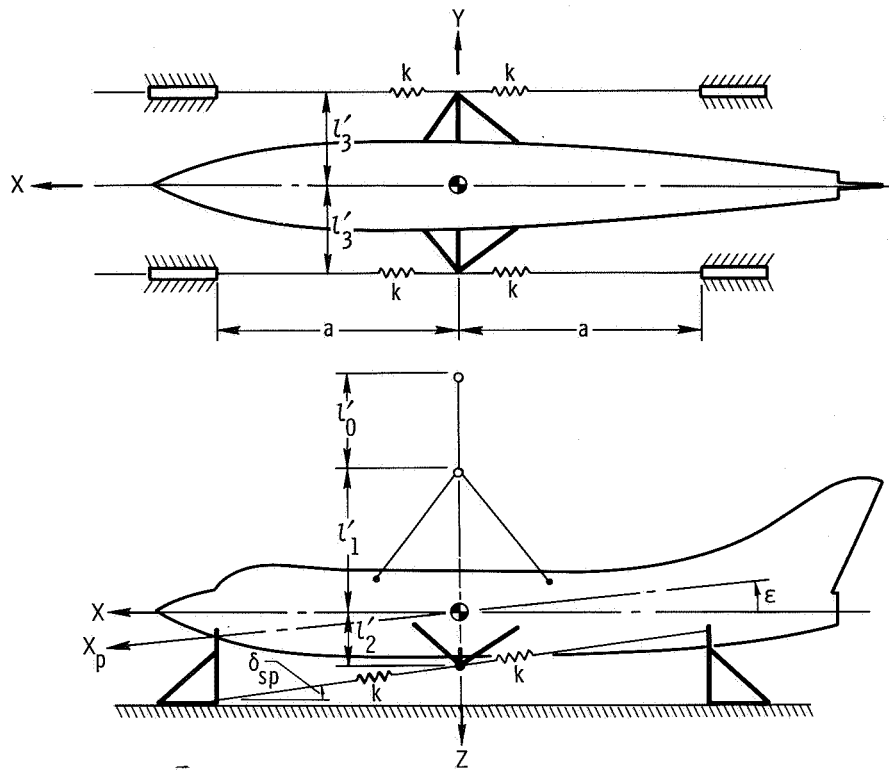
(a) Test setup.
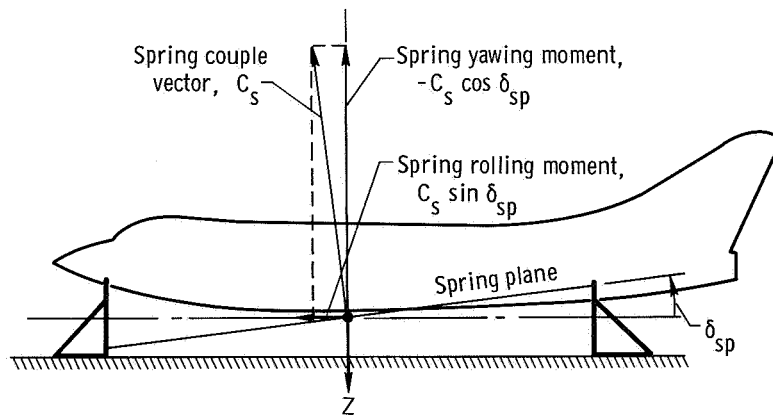
(b) Resolution of spring couple vector.

Figure 11. Test setup and resolution of spring couple vector in single-point suspension method for determining the yawing moment of inertia, the product of inertia, and the inclination of the principal axis.

Objective and Principle of the Method

The objective of the single-point suspension method is to determine the inclination of the spring plane at which the roll-to-yaw ratio of the yaw mode of oscillation is zero. After this inclination and the corresponding frequency of the yaw mode of oscillation have been determined, the yawing moment of inertia, the inclination of the principal axis, and the product of inertia can be determined.

In principle, as outlined in reference 7, the method considers a pure yaw-mode response to a yaw excitation. With the spring plane at some one inclination, δ_{sp} (fig. 11(b)), a yaw-mode excitation of the aircraft results in a certain amount of oscillatory roll response as well as yaw response. The restoring spring couple vector, C_s (fig. 11(b)), produces a restraining moment on the yaw motion and a rolling moment that either reinforces or restrains the rolling moment, depending on the inclination of the vector. The yaw-mode transient responses in roll and yaw, following yaw excitation, are represented by the following equations:

$$I_X \dot{p} - I_{XZ} \dot{r} = C_s \sin \delta_{sp} \tag{21a}$$

$$I_Z \dot{r} - I_{XZ} \dot{p} = -C_s \cos \delta_{sp} \tag{21b}$$

At some one value of δ_{sp} the rolling motion of the yaw mode will be zero. At this condition $\varphi = 0$ and thus $\dot{p} = 0$, and the equations reduce to

$$-I_{XZ} \dot{r} = C_s \sin \left(\delta_{sp} \right)_{\varphi=0} \tag{22a}$$

$$I_Z \dot{r} = -C_s \cos \left(\delta_{sp} \right)_{\varphi=0} \tag{22b}$$

Hence, when $\varphi = 0$ and thus $\dfrac{|p|}{|r|}\bigg|_{\psi} = 0$,

$$\tan \left(\delta_{sp} \right)_{\varphi=0} = \frac{I_{XZ}}{I_Z} \tag{23}$$

and

$$I_{XZ} = I_Z \tan \left(\delta_{sp} \right)_{\varphi=0} \tag{24}$$

Since the inclination of the principal pitch axis for a symmetrical airplane is given by the expression

$$\tan 2\varepsilon = \frac{2 I_{XZ}}{I_Z - I_X} \tag{25}$$

where ε is the inclination of the principal axis relative to the horizontal reference X-axis, substituting equation (24) into equation (25) gives

$$\tan 2\varepsilon = \frac{2I_z \tan \left(\delta_{sp}\right)_{\varphi=0}}{I_z - I_X} \tag{26}$$

The yawing moment of inertia can readily be determined as a byproduct of this method. Using equation (22b) and considering δ_{sp} to be the angle at which $\dfrac{|\varphi_1|}{|\psi|_\psi} = 0$,

$$I_z = \frac{-C_s \cos \left(\delta_{sp}\right)_{\varphi=0}}{\dot{r}} \tag{27}$$

With the springs configured longitudinally, as in figure 11(a), C_s for $\dfrac{|\varphi|}{|\psi|_\psi} = 0$ is represented by the expression

$$C_s = \left[4k\left(\ell'_3\right)^2 \cos \left(\delta_{sp}\right)_{\varphi=0} \right] \psi \tag{28}$$

and $\dot{r}$ is represented by $-\psi\left(\omega_\psi\right)^2$. Substituting these expressions into equation (27) results in

$$I_z = \frac{4k\left(\ell'_3\right)^2 \cos \left(\delta_{sp}\right)_{\varphi=0}}{\left(\omega_\psi\right)^2} \tag{29}$$

Response Characteristics of the Actual System

A simple yaw and roll motion response to a yaw-mode excitation at the yaw-mode frequency would be ideal for the single-point suspension method. Actually, the system allows the aircraft to rotate about all three axes and to translate along the pitch and roll axes. The proper application of excitation can eliminate the longitudinal motion in a lateral excitation; however, the yaw mode, the rocking mode, and the sway mode of oscillation (fig. 12) must be accounted for.

The yaw mode is primarily a yawing motion at the yaw-mode frequency, with some coupled roll motion and a small amount of sidewise motion. The yaw mode is required for the determination of I_{XZ} and I_Z.

The rocking mode, ideally, is a rolling motion at rocking-mode frequency without sidewise or yaw motion. Actually, it may contain a small amount of sidewise and yaw motion. The unintentional excitation of this mode during the excitation of the yaw mode produces a significant and unwanted interference with the roll response of the yaw mode in recorded time histories. This interference can be accounted for in the analysis of the response data.
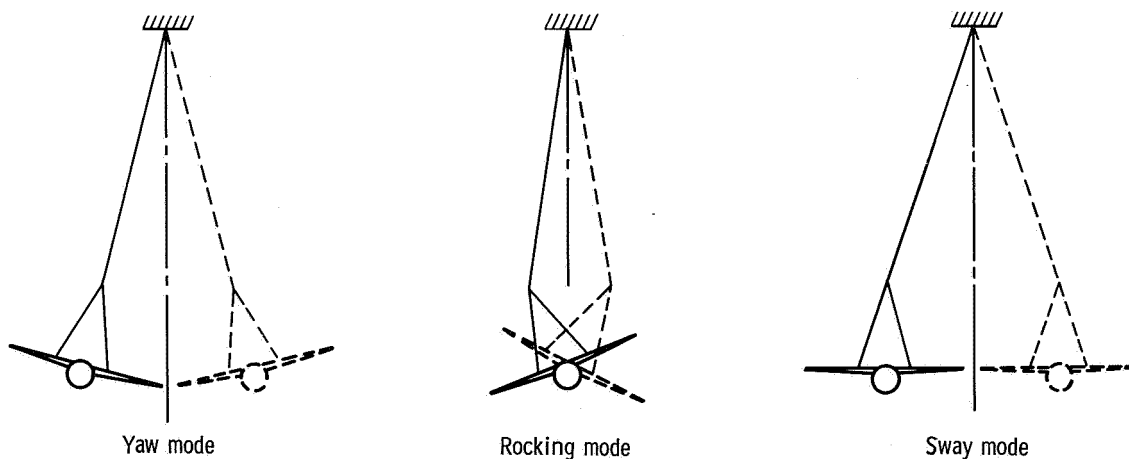
Yaw mode   Rocking mode   Sway mode

Figure 12. Rolling motions of the three natural modes of oscillation to be accounted for in responses to yaw-mode excitation in the single-point suspension method for determining the product of inertia and the inclination of the principal axis. Motions are exaggerated for clarity.

The sway mode is primarily a sidewise motion at the sway-mode frequency, where it usually contains some roll motion and a negligible amount of yaw motion. The interference of the sway-mode roll motion with the yaw-mode roll motion can be made negligible by proper design of the suspension rig.

Since the roll-to-yaw ratio and the frequency of oscillation of the yaw mode are the desired response characteristics, and should be accounted for quantitatively as a function of the inclination of the spring plane, it is essential to obtain a mathematical insight into the interacting effects of the three modes of oscillation on the frequency of oscillation and amplitude ratio of the yaw mode. This insight enhances the minimization and isolation of the interference of the rocking and sway modes with the yaw-mode characteristics.

Equations of motion. — The following spring forces and moments, which are used in the equations of motion, are based on a small-perturbation analysis of the longitudinal configuration of the springs and the schematics of the suspension system shown in figures 11(a) and 13. Experience has
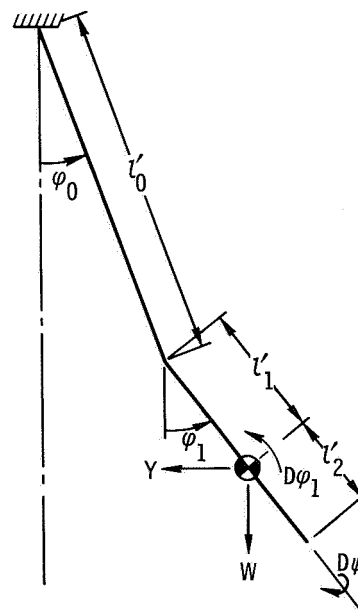

Figure 13. Schematic diagram of small-perturbation motions and gravitation force in single-point suspension system.

shown that since the distance from the spring attachment point at the airplane to the spring stanchion (distance a in fig. 11(a)) is of the order of 3.5 meters to 4.5 meters, the spring side forces are normally negligible in comparison with the side component of the gravitational force. Similarly, the spring moments due to the spring side forces are negligible in comparison with the spring moments due to angular motions. Thus, for the purposes of the present study,

$$Y_s \approx 0 \tag{30}$$

$$L_s \approx \left(k_t \cos \delta_{sp} \sin \delta_{sp}\right)\psi - \left(k_t \sin^2 \delta_{sp}\right)\varphi_1 \tag{31}$$

$$N_s \approx \left(k_t \cos \delta_{sp} \sin \delta_{sp}\right)\varphi_1 - \left(k_t \cos^2 \delta_{sp}\right)\psi \tag{32}$$

where

$$k_t = 4k\left(\ell_3'\right)^2 \tag{33}$$

The contributions of the gravitational and inertial forces and moments to the equations of motion are obtained by using Lagrangian equations and figure 13. The following equations of motion can then be obtained by combining the spring with the gravitational and inertial contributions:

$$
\begin{bmatrix}
W\dfrac{\ell_1'}{\ell_0'} & 0 & \dfrac{W}{g}\left(D^2 + \dfrac{g}{\ell_0'}\right) \\[3ex]
I_X D^2 + W\ell_1\left(1 + \dfrac{\ell_1'}{\ell_0'}\right) & -I_{XZ}D^2 & W\dfrac{\ell_1'}{\ell_0'} \\[3ex]
-I_{XZ}D^2 & I_Z D^2 & 0
\end{bmatrix}
\begin{vmatrix} \varphi_1 \\[3ex] \psi \\[3ex] y \end{vmatrix}
=
\begin{vmatrix} Y_s \\[3ex] L_s \\[3ex] N_s \end{vmatrix}
\qquad
\begin{matrix}(34a)\\[3ex](34b)\\[3ex](34c)\end{matrix}
$$

By substituting equations (30), (31), and (32) for Y_s, L_s, and N_s, respectively, and consolidating,

$$
\begin{bmatrix}
A & 0 & \dfrac{W}{g}\left[D^2 + \left(\omega_y\right)_0^2\right] \\[3ex]
I_X\left[D^2 + \left(\omega_\varphi\right)_0^2\right] & -I_{XZ}\left[D^2 + p_1^2\right] & A \\[3ex]
-I_{XZ}\left[D^2 + p_1^2\right] & I_Z\left[D^2 + \left(\omega_\psi\right)_0^2\right] & 0
\end{bmatrix}
\begin{vmatrix} \varphi_1 \\[3ex] \psi \\[3ex] y \end{vmatrix}
= 0
\qquad
\begin{matrix}(35a)\\[3ex](35b)\\[3ex](35c)\end{matrix}
$$

where

$$A = W \frac{\ell'_1}{\ell'_0} \tag{36}$$

$$p_1^2 = \frac{k_t}{I_{XZ}} \cos \delta_{sp} \sin \delta_{sp} \tag{37}$$

$$\left(\omega_y\right)_0^2 = \frac{g}{\ell'_0} \tag{38}$$

$$\left(\omega_\varphi\right)_0^2 = \left[W\ell'_1\left(1 + \frac{\ell'_1}{\ell'_0}\right) + k_t \sin^2 \delta_{sp} \right]\frac{1}{I_X} \tag{39}$$

$$\left(\omega_\psi\right)_0^2 = \frac{k_t}{I_Z} \cos^2 \delta_{sp} \tag{40}$$

Yaw-mode frequency. — From the matrix of equations (35), the characteristic equation can readily be determined to be

$$\left[D^2 + \left(\omega_\varphi\right)_0^2\right]\left[D^2 + \left(\omega_\psi\right)_0^2\right]\left[D^2 + \left(\omega_y\right)_0^2\right] - \frac{I_{XZ}^2}{I_X I_Z}\left[D^2 + p_1^2\right]^2\left[D^2 + \left(\omega_y\right)_0^2\right] - \frac{A^2}{\frac{W}{g}I_X}\left[D^2 + \left(\omega_\psi\right)_0^2\right] = 0 \tag{41}$$

A direct solution of equation (41), for yaw-mode frequency, is complex. A simpler solution, described in reference 8, considers a mode frequency on the basis of

$$\omega^2 = \omega_0^2 + \Delta\omega^2 \tag{42}$$

Thus, to obtain the yaw-mode frequency, ω_ψ, from the characteristic equation, let $D^2 = -\left(\omega_\psi\right)^2 = -\left(\omega_\psi\right)_0^2 - \Delta\left(\omega_\psi\right)^2$. The resulting solution gives the following expression for $\Delta\left(\omega_\psi\right)^2$:

$$\Delta\left(\omega_\psi\right)^2 = \cfrac{\cfrac{I_{XZ}^2}{I_X I_Z}\cfrac{\left[\left(\omega_\psi\right)^2 - p_1^2\right]^2}{\left[\left(\omega_\psi\right)^2 - \left(\omega_\varphi\right)_0^2\right]}}{1 - \cfrac{A^2}{\frac{W}{g}I_X\left[\left(\omega_\psi\right)^2 - \left(\omega_\varphi\right)_0^2\right]\left[\left(\omega_\psi\right)^2 - \left(\omega_y\right)_0^2\right]}} \tag{43}$$

At the expense of a small error in $\Delta\left(\omega_\psi\right)^2$, $\left(\omega_\psi\right)_0^2$ can be substituted for $\left(\omega_\psi\right)^2$ in the equation.

Equation (43) indicates that the yaw-mode frequency is affected to some extent by the uncoupled roll-mode frequency, $\left(\omega_\varphi\right)_0^2$, and the uncoupled sway-mode frequency, $\left(\omega_y\right)_0^2$, except at the one condition pertinent to the experimental investigation. When p_1^2 equals $\left(\omega_\psi\right)^2$, which is the condition required for the yaw-mode amplitude ratio, $\dfrac{|\varphi_1|}{|\psi|_\psi}$, to be zero (as shown later), $\Delta\left(\omega_\psi\right)^2$ equals zero and the yaw-mode frequency is simply $\left(\omega_\psi\right)_0^2$, which is the frequency of a simple uncoupled yaw motion. This is fortunate, since this uncoupled frequency, obtained experimentally, is required for the accurate determination of the yawing moment of inertia, which is essential in obtaining the product of inertia.

Amplitude ratios. — The roll-to-yaw amplitude ratio of the yaw mode is obtained from equation (35b) after substituting equation (35a) for y in equation (35b) and letting D^2 equal $-\left(\omega_\psi\right)^2$. Thus,

$$\frac{|\varphi_1|}{|\psi|_\psi} = \cfrac{\dfrac{I_{XZ}}{I_X I_Z}\dfrac{\left[\left(\omega_\psi\right)^2 - p_1^2\right]}{\left[\left(\omega_\psi\right)^2 - \left(\omega_\varphi\right)_0^2\right]}}{1 - \cfrac{A^2}{\dfrac{W}{g}I_X\left[\left(\omega_\psi\right)^2 - \left(\omega_\varphi\right)_0^2\right]\left[\left(\omega_\psi\right)^2 - \left(\omega_y\right)_0^2\right]}} \tag{44}$$

Equation (44) indicates that there should be a significant difference between the magnitude of $\left(\omega_\psi\right)^2$ and that of $\left(\omega_\varphi\right)_0^2$. In addition, the equation indicates that when p_1^2 equals $\left(\omega_\psi\right)^2$, the amplitude ratio $\dfrac{|\varphi_1|}{|\psi|_\psi}$ is zero. At this condition, with the corresponding inclination angle, δ_{sp}, of the spring plane and the uncoupled yaw-mode frequency, $\left(\omega_\psi\right)_0$, known from experimental data, the yawing moment of inertia is obtained from equation (40) and the product of inertia is obtained by equating equations (37) and (40). Thus,

$$I_Z = \frac{k_t \cos^2\left(\delta_{sp}\right)_{\varphi=0}}{\left(\omega_\psi\right)_0^2} \tag{45}$$

and

$$I_{XZ} = I_Z \tan \left(\delta_{sp}\right)_{\varphi=0} \tag{24}$$

The roll-to-yaw amplitude ratio of the rocking mode is obtained from equation (35c) with D^2 equal to $-\left(\omega_\varphi\right)^2$. Thus,

$$\frac{\left|\varphi_1\right|}{\left|\psi\right|_\varphi} = \frac{I_Z}{I_{XZ}} \frac{\left[\left(\omega_\psi\right)_0^2 - \left(\omega_\varphi\right)^2\right]}{\left[p_1^2 - \left(\omega_\varphi\right)^2\right]} \tag{46}$$

Equation (46) indicates that the rolling motion of the rocking mode can be eliminated by making $\left(\omega_\psi\right)_0^2$ equal to $\left(\omega_\varphi\right)^2$ to avoid possible interference of this rolling motion with the roll response of the yaw mode. However, this is not feasible, since it conflicts with the yaw-mode requirement of equation (44) for a good amount of separation between $\left(\omega_\psi\right)^2$ and $\left(\omega_\varphi\right)_0^2$. For the critical condition of the yaw mode $\frac{\left|\varphi_1\right|}{\left|\psi\right|_\psi} = 0$, at which condition p_1^2 equals $\left(\omega_\psi\right)_0^2$, equation (46) reduces to

$$\frac{\left|\varphi_1\right|}{\left|\psi\right|_\varphi} = \frac{I_Z}{I_{XZ}} \tag{47}$$

At this critical condition, the rocking mode has a high roll-to-yaw ratio that is determined by the inertial characteristics alone. The amplitude of the rocking-mode roll motion, $\left|\varphi_1\right|_\varphi$, is dependent upon the amplitude of the rocking-mode yaw motion, $\left|\psi\right|_\varphi$, unintentionally induced during the excitation of the yaw mode.

For the sway mode, the amplitude ratios $\frac{\left|\varphi_1\right|}{\left|-y\right|_y}$ and $\frac{\left|\psi\right|}{\left|-y\right|_y}$ are the ratios of interest in obtaining insight into sway-mode interference with the yaw-mode amplitude ratio, $\frac{\left|\varphi_1\right|}{\left|\psi\right|_\psi}$. The following expression for $\frac{\left|\varphi_1\right|}{\left|-y\right|_y}$ can be obtained from equations (35) with D^2 approximately equal to $-\left(\omega_y\right)_0^2$:

$$\frac{\left|\varphi_1\right|}{\left|-y\right|_y} \approx \frac{A}{I_X\left[\left(\omega_\varphi\right)_0^2 - \left(\omega_y\right)_0^2\right]} \tag{48}$$

Substituting equations (36), (38), and (39) for A, $\left(\omega_y\right)_0^2$, and $\left(\omega_\varphi\right)_0^2$,

respectively, results in

$$\frac{|\varphi_1|}{|-y|_y} \approx \frac{1}{\left(\ell_0' + \ell_1'\right) + \dfrac{k_t \sin^2 \delta_{sp}}{W\left(\dfrac{\ell_1'}{\ell_0'}\right)} - \dfrac{gI_X}{W\ell_1'}} \tag{49}$$

Since the amplitude of the sway-mode rolling motion, $\left|\varphi_1\right|_y$, is primarily dependent upon both $\ell_0' + \ell_1'$ and the amplitude of the sway-mode sidewise motion, $\left|-y\right|_y$, the minimization of this unwanted motion is dependent upon the care taken to avoid exciting the sway mode during the excitation of the yaw mode as well as upon the magnitude of $\ell_0' + \ell_1'$.

The sway-mode amplitude ratio, $\dfrac{|\psi|}{|-y|_y}$, can also be obtained from equations (35b) and (35c) with D^2 approximately equal to $-\left(\omega_y\right)_0^2$:

$$\frac{|\psi|}{|-y|_y} \approx \left(\frac{AI_{XZ}}{I_X I_Z}\right) \frac{\left[p_1^2 - \left(\omega_y\right)_0^2\right]}{\left[\left(\omega_\psi\right)_0^2 - \left(\omega_y\right)^2\right]\left[\left(\omega_\varphi\right)_0^2 - \left(\omega_y\right)_0^2\right]} \tag{50}$$

For the critical condition of the yaw mode, $\dfrac{|\varphi_1|}{|\psi|_\psi} = 0$, at which condition $p_1^2 = \left(\omega_\psi\right)_0^2$,

$$\frac{|\psi|}{|-y|_y} \approx \left(\frac{AI_{XZ}}{I_X I_Z}\right) \frac{1}{\left[\left(\omega_\varphi\right)_0^2 - \left(\omega_y\right)_0^2\right]} \tag{51}$$

or

$$\frac{|\psi|}{|-y|_y} \approx \frac{I_{XZ}}{I_Z} \left[\frac{1}{\left(\ell_0' + \ell_1'\right) + \dfrac{k_t \sin^2 \delta_{sp}}{W\dfrac{\ell_1'}{\ell_0'}} - \dfrac{gI_X}{W\ell_1'}}\right] \tag{52a}$$

43

$$\frac{|\psi|}{|-y|} \approx \frac{I_{XZ}}{I_Z} \frac{1}{(\ell_0' + \ell_1')} \qquad (52b)$$

For this condition, the sway-mode yaw amplitude is negligible. It can also be considered to be negligible for conditions other than the critical condition.

As indicated by the preceding discussion, the sway-mode yawing motion is negligible and will not interfere with obtaining yaw-mode roll-to-yaw ratios from experimental time histories. The sway-mode rolling motion can also be reduced to negligibility by proper suspension system design. The minimization of the rocking-mode rolling and yawing motions depends primarily upon the technique used to excite the yaw-mode motions. When rocking-mode rolling and yawing motions are present in experimental time histories, it is relatively simple to isolate them to obtain the desired yaw-mode data.

Minimization of the sway mode. — To minimize the effects of the sway-mode rolling motion on the total rolling motion in attempting to obtain yaw-mode responses, the sway-mode amplitude ratio, $\frac{|\varphi_1|}{|-y|_y}$, and the amplification factor, $\frac{|y|}{|y_{st}|}$, must be minimized, since

$$\frac{|\varphi_1|}{|-y_{st}|_y} = \frac{|\varphi_1|}{|-y|_y} \frac{|y|}{|y_{st}|} \qquad (53)$$

Reference 8 suggests that $\frac{|\varphi_1|}{|-y|_y}$ should be less than 0.164 radian per meter to prevent the sway-mode rolling motion from having significant effect on the total rolling motion. Using this as a criterion and applying it to equation (48),

$$0.164 > \frac{A}{I_X\left[\left(\omega_\varphi\right)_0^2 - \left(\omega_y\right)_0^2\right]} \qquad (54)$$

By substituting equations (36), (38), and (39) for A, $\left(\omega_y\right)_0^2$, and $\left(\omega_\varphi\right)_0^2$, respectively, equation (54) can be used to solve for $\ell_0' + \ell_1'$ for a selected value of ℓ_1':

$$\ell_0' + \ell_1' > 6.1 - \frac{k_t \sin^2 \delta_{sp}}{W \dfrac{\ell_1'}{\ell_0'}} + \frac{g}{\ell_1'} \frac{W}{I_X} \qquad (55)$$

The first term in equation (55) is dominant. At the NASA Flight Research Center,

44

inertia experiments are normally conducted with a value of $\ell'_0 + \ell'_1$ of approximately 7.5 meters. This is in accord with the criterion.

The expression for the amplification factor $\dfrac{|y|}{|y_{st}|}$ is obtained by introducing a sinusoidal exciting side force, Y_F, applied at the yaw-mode frequency, into equation (35a) and considering the yaw angle to be equal to zero in the rolling-moment equation (eq. (35b)). The exciting force is considered to be so positioned as not to excite the rocking mode. Thus equation (35a) becomes

$$A\varphi_1 + \left(mD^2 + k_y\right)y = Y_F \tag{56a}$$

and equation (35b) becomes

$$I_X\left[D^2 + \left(\omega_\varphi\right)_0^2\right]\varphi_1 + Ay = 0 \tag{56b}$$

With D^2 equal to $-\left(\omega_\psi\right)^2$, where ω_ψ is the exciting frequency, and y_{st} equal to $\dfrac{Y_F}{k_y}$, the following equation can be obtained:

$$\frac{|\overline{y}|}{|y_{st}|} = \cfrac{1}{-\cfrac{A\ell'_1}{I_X\left[\left(\omega_\varphi\right)_0^2 - \left(\omega_\psi\right)_0^2\right]} + \left[1 - \cfrac{\left(\omega_\psi\right)^2}{\left(\omega_y\right)^2}\right]} \tag{57a}$$

or

$$\frac{|y|}{|y_{st}|} \approx \cfrac{1}{-\cfrac{\ell'_1}{\ell'_0 + \ell'_1 - \cfrac{I_X g\left(\omega_\psi\right)^2}{W\left(\omega_y\right)_0^2}} + \left[1 - \cfrac{\left(\omega_\psi\right)^2}{\left(\omega_y\right)^2}\right]} \tag{57b}$$

It is apparent that the attenuation of $\dfrac{|y|}{|y_{st}|}$ requires $\left(\omega_\psi\right)^2$ to be much greater than $\left(\omega_y\right)_0^2$. This condition is readily satisfied, since $\left(\omega_\psi\right)^2$ is normally greater than 12 and $\left(\omega_y\right)_0^2$, which is equal to $\dfrac{g}{\ell'_0}$, can be made desirably smaller by making

ℓ'_0 as long as possible or ℓ'_1 as short as possible.

The effects of the sway mode on total rolling motion can be reduced further by minimizing the excitation of y_{st}. This can be done by gradually building up a sinusoidal yaw motion at the yaw-mode frequency with an exciting force that is kept small by placing it as far forward or rearward of the center of gravity as possible.

Minimization and isolation of the rocking-mode rolling motions. — If the vertical positioning of the exciting force is improper during the excitation of the yaw mode, the exciting force may also excite the rocking mode. The factors that affect the response of the rocking-mode rolling motion to a lateral force that excites the yaw mode at the yaw-mode natural frequency can be obtained from the following approximation of the rolling-moment equation:

$$I_X \left[D^2 + \left(\omega_\varphi \right)_0^2 \right] \varphi_1 \approx L_F \tag{58}$$

where

$$L_F = k_\varphi \varphi_{st} \tag{59}$$

With D^2 equal to $-\left(\omega_\psi \right)^2$, where ω_ψ is the exciting frequency, the following expression can be obtained from equation (58):

$$\left| \varphi_1 \right|_\varphi = \frac{\varphi_{st}}{\dfrac{I_X \left(\omega_\varphi \right)_0^2}{k_\varphi} \left[1 - \dfrac{\left(\omega_\psi \right)^2}{\left(\omega_\varphi \right)_0^2} \right]}$$

which reduces to

$$\left| \varphi_1 \right|_\varphi = \frac{\varphi_{st}}{1 - \dfrac{\left(\omega_\psi \right)^2}{\left(\omega_\varphi \right)_0^2}} \tag{60}$$

Equation (60) indicates that the rolling motion of the rocking mode can be attenuated by minimizing φ_{st} and also by making $\dfrac{\left(\omega_\psi \right)^2}{\left(\omega_\varphi \right)_0^2}$ much greater than 2. Since

46

φ_{st} is equal to $\dfrac{L_F}{k_\varphi}$, the minimization of φ_{st} depends upon keeping the yaw-mode exciting force as small as possible and positioning this force properly. Attenuating the rolling motion of the rocking mode by making $\dfrac{\left(\omega_\psi\right)^2}{\left(\omega_\varphi\right)_0}$ much greater than 2 may not be desirable because of the possibility of exciting structural modes of vibration, which should be avoided. In addition, $\left(\omega_\psi\right)^2$ should be dissimilar to $\left(\omega_\varphi\right)_0^2$, since equation (44) indicates that a well-defined difference is necessary if the yaw mode $\dfrac{|\varphi_1|}{|\psi|}\bigg|_\psi$, or its equivalent, $\dfrac{|p|}{|r|}\bigg|_\psi$, is to be determined. At the NASA Flight Research Center, it has been the practice to make $\dfrac{\left(\omega_\psi\right)^2}{\left(\omega_\varphi\right)_0^2}$ approximately equal to 0.5 to avoid the excitation of structural modes of vibration as well as to provide a reasonable separation between the two frequencies.

From the preceding discussions of the single-point suspension, it is obvious that the frequencies of the sway mode, rocking mode, and yaw mode should be separated by a significant amount by the design of the suspension system. Also, the excitation of the yaw mode should be sinusoidal and performed in a way that does not excite the rocking mode. In addition, the damping of the responses should be negligible. Finally, if the suspension system is properly installed, the roll-rate and yaw-rate responses (the responses normally recorded) are in phase or 180° out of phase.
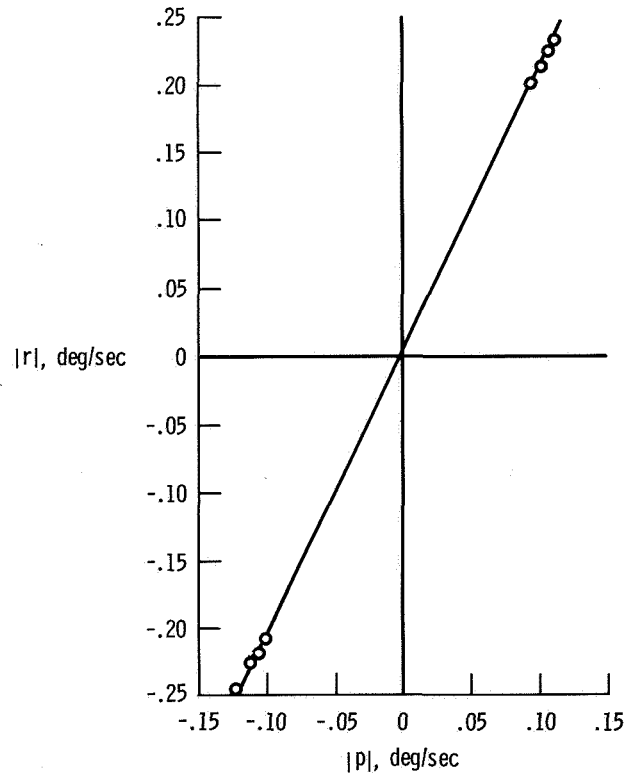
When rocking-mode rolling and yawing motions cannot be avoided, and are therefore present in the total response to yaw excitation, they can be isolated from the total motion in the time histories (provided that the sway-mode motions are insignificant), and the yaw-mode roll-to-yaw ratio can be obtained by plotting the peak values of the roll rate against the peak values of the yaw rate. In essence, this constitutes plotting the bounding outline of a lissajous figure. (Lissajous figures are discussed in detail in reference 8.) As shown below, this method of identifying and eliminating the rocking-mode motion from time histories to obtain the yaw mode can be applied even if significant damping is present.

Figure 14(a) shows time histories of roll-rate and yaw-rate responses to yaw-mode excitation in which the rocking-mode interference with the yaw-mode rolling motion was absent but damping was present. A cross plot of the peaks of roll rate plotted against the peaks of yaw rate (to obtain the $\dfrac{|p|}{|r|}\bigg|_\psi$ of the yaw mode) is shown in figure 14(b). Because of the absence of rocking-mode interference with the yaw-mode responses, the cross plot shows only a single line. Also, because of the damping, there are several points along the line; if damping had not been present, the line would have been defined by only two points, one at each end.
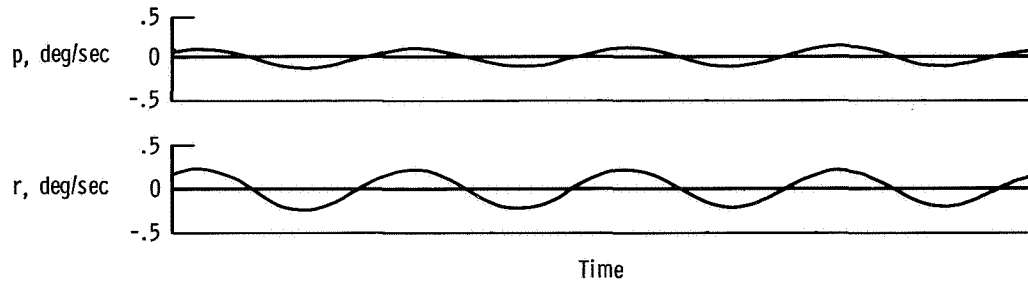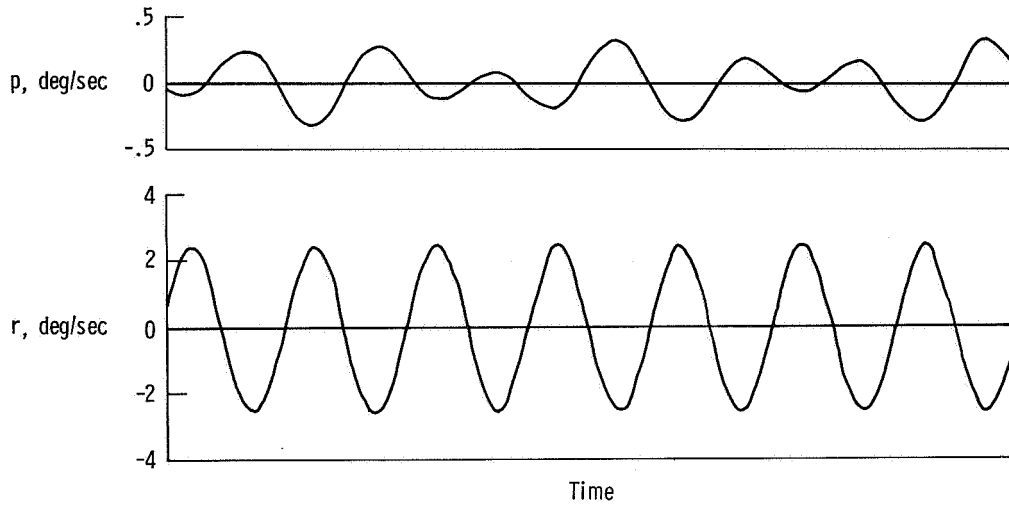
(a) Time histories of transient responses.

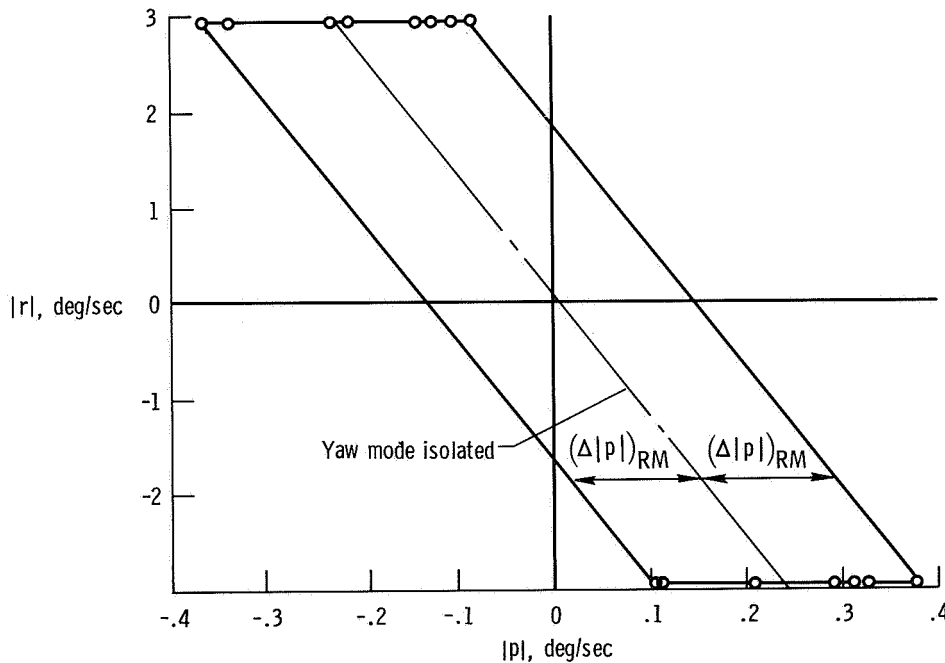(b) Lissajous cross plot; $\dfrac{|p|}{|r|}_{\psi} = 0.485.$

Figure 14. Time histories and lissajous cross plot of a lightly damped transient response free of rocking- and sway-mode interference after yaw-mode excitation.

When the rolling motion of the rocking mode interferes with the rolling motion of the yaw mode and damping is negligible, the time histories of roll- and yaw-rate responses are like those in figure 15(a) (from ref. 8). A cross plot of the peaks of these roll-rate and yaw-rate responses results in a lateral spread of the points, as shown in figure 15(b). Drawing a boundary outline of the points, as shown in this figure, produces a parallelogram that is the bounding outline of a lissajous figure. The mean line of the left and right sides of the parallelogram represents the response

of the yaw mode. The slope of this line is the amplitude ratio of the yaw mode, $\frac{|p|}{|r|}\bigg|_\psi$, for the tilt angle of the spring plane, δ_{sp}. The lateral distance from this mean line to the side of the parallelogram is the amplitude due to the rocking mode, $|p|_\varphi$.
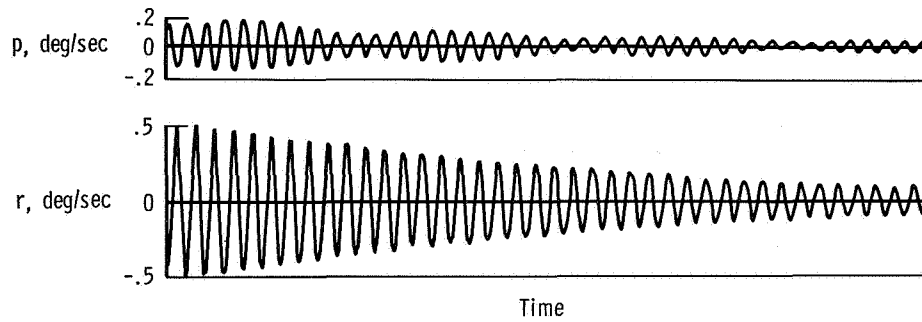

(a) Time histories of transient responses (from ref. 8).
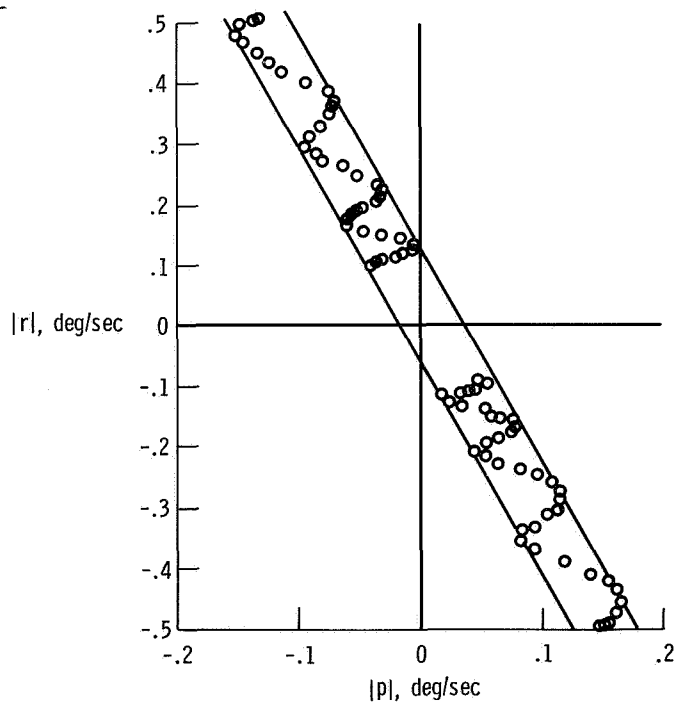

(b) Lissajous cross plot; $\frac{|p|}{|r|}\bigg|_\psi = 0.078$.

Figure 15. Time histories and lissajous cross plot of a transient response after yaw-mode excitation. Rocking-mode roll-rate interference; no damping.

49

When the rolling motion of the rocking mode interferes with the response to yaw-mode excitation and light damping is present, as in the time histories in figure 16(a), a cross plot of the roll and yaw time histories results in an oscillatory curve like that in figure 16(b). Although the curve is oscillatory, the bounding lines of the left and right side are parallel and constitute the bounds of the lissajous figure with damping present. As in figures 14(b) and 15(b), the slope of the bounding lines is the roll-to-yaw ratio of the yaw mode for the tilt angle of the spring plane, δ_{sp}.

(a) Time histories of transient responses.

(b) Lissajous cross plot; $\dfrac{|p|}{|r|}\bigg|_{\psi} = 0.284$.

Figure 16. Time histories and lissajous cross plot of a transient response after yaw-mode excitation, with damping and interference from rocking mode.

50

Practical Considerations in Setting Up the Experiment
and Exciting the Yaw Mode

The experimental installation must be set up so that it provides rigidity in the suspension sling and spring attachment provisions, minimizes spring sag, minimizes damping, and provides adequately sensitive onboard response sensors. The method used to excite the yaw mode should minimize the excitation of the sway and rocking modes.

The suspension sling should constitute, in effect, a rigid system between the vehicle and the point of suspension. The point of suspension at the end of the suspension line should constitute a single-point pivot. Single-point pivot action is essential to the determination of the vertical center-of-gravity position by the single-point suspension method.

The pylons or outrigger assembly used to attach the springs to the vehicle must be rigid relative to the reference axis system. Elasticity in the assembly relative to the reference axes results in secondary spring action in series with the regular springs, which makes a softer effective spring than intended. Figure 17 shows the suspension configuration used for the HL-10 lifting body vehicle, and
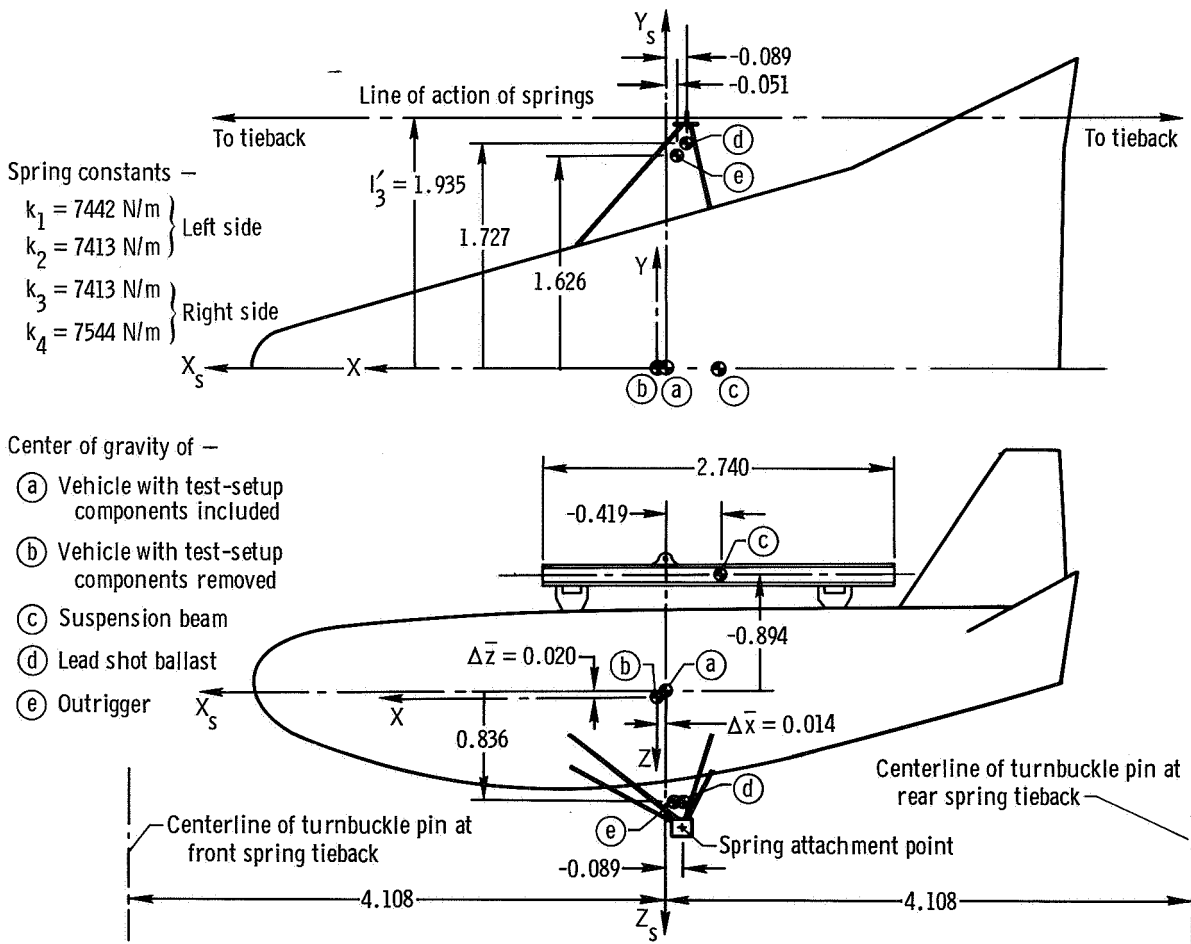

Figure 17. Configuration of HL-10 lifting body vehicle for the determination of I_Z, I_{XZ}, and ε. All dimensions are in meters.

figure 18 shows the spring attachment provisions used to swing the vehicle. The rigidity of the spring attachment outrigger relative to the reference axes is evident in the photograph.
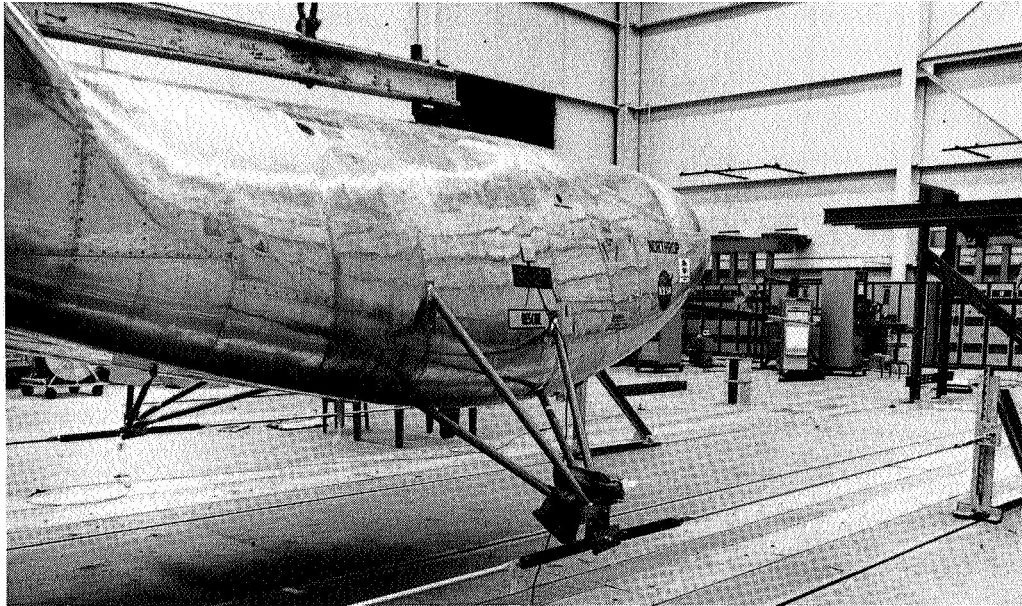

Figure 18. Single-point suspension of the HL-10   E-14687
lifting body vehicle showing spring attachment
provisions, including spring mounting plate with
spherical bearing.

To enhance the freedom of action of the springs at the attachment point during rolling and yawing motions, a spring mounting plate with a spherical bearing was fabricated (fig. 18). The tieback from the spring to the stanchion should be as light as possible to minimize sag in the line of action of the springs. It should also be longitudinally rigid to prevent secondary spring action in series with the actual spring. Therefore, flexible cables should not be used. Lightweight aluminum tubing with swaged ends is effective.

Since the spring and the turnbuckle are heavy, care must be taken to minimize sag in the line from the spring attachment point to the tieback stanchion. The spring should be pretensioned enough to prevent obvious sag in the line of action during periods of motion when the spring tension is relaxed.

Before the springs are installed, a plumb bob should be used to find the position of the spring attachment points on the ground. After the springs are attached and pretensioned, and after each change in the inclination of the spring plane, the spring attachment point should remain in the original position. This prevents forward or rearward displacement in the suspension and change in the pitch attitude.

The vehicle should be leveled laterally as well as longitudinally by using a clinometer and ballast. Figure 18 shows the lead shot ballast used to level the HL-10 lifting body vehicle. This weight is accounted for in figure 17.

The electric lines that connect the onboard sensors with the remote recorders should be for pertinent sensors only, and they should be suspended so that damping of the vehicle's motion is minimized.

The yaw mode should be excited without inadvertently exciting the pitch mode. Pitch rate as well as roll and yaw rates should be recorded to check for pitch-mode excitation. In addition, the excitation of the sway mode should be minimized and the excitation of the rocking mode should be minimized or avoided. At the NASA Flight Research Center, the yaw mode is excited by gradually building up a sinusoidal force that is applied at the yaw-mode frequency as far forward as possible. The force is positioned vertically so that the tendency to excite the rocking mode is minimized. One technique that can be used to apply the force is to extend the left and right index fingers laterally and apply them at the horizontal diameter of the nose boom or to a vertical plate attached to the vehicle. An oscilloscope arranged to show the lissajous figure responses of roll and yaw rates is useful for learning the technique. The optimum application of the exciting force and the transient responses appears on the oscilloscope as a sloped straight line.

Reduction of Experimental Data To Find Yawing Moment of Inertia, Product of Inertia, and Inclination of Principal Axis

Data for the HL-10 lifting body vehicle are used to illustrate the reduction of experimental data to obtain the yawing moment of inertia, product of inertia, and inclination of the principal axis. The portion of the experiment that deals with the determination of the vertical and horizontal position of the center of gravity is summarized in appendix A.

Figure 17 shows the experimental configuration of the vehicle, the center-of-gravity positions of the vehicle for the test-setup and clean conditions, and the center-of-gravity locations of the test equipment. Figure 19 shows the experimentally determined variation of $\frac{|p|}{|r|}_\psi$ and the period of oscillation as a function of δ_{sp} for the test setup. At the point where $\frac{|p|}{|r|}_\psi = 0$, the data indicate that δ_{sp} is known within $\pm 0.1°$. It should be noted that the $\frac{|p|}{|r|}_\psi$ curve is not necessarily a straight line. Therefore, if only a few data points had been obtained (for the outlying ends of the curve), it would have been invalid to assume the presence of a hysteresis effect defined by straight lines depicting the upper and lower bounds of the data.

With ω_ψ and δ_{sp} known for the condition where $\frac{|p|}{|r|}_\psi = 0$, the yawing moment of inertia, the product of inertia, and the inclination of the principal axis were determined as shown in appendix B. The yawing moment of inertia for the experimental setup was obtained first. This value was then corrected for the effects of the experimental rig and the inertial effects of the apparent additional air mass. The air mass effects, which were calculated using the procedures in reference 11, are significant, as indicated in appendix B.
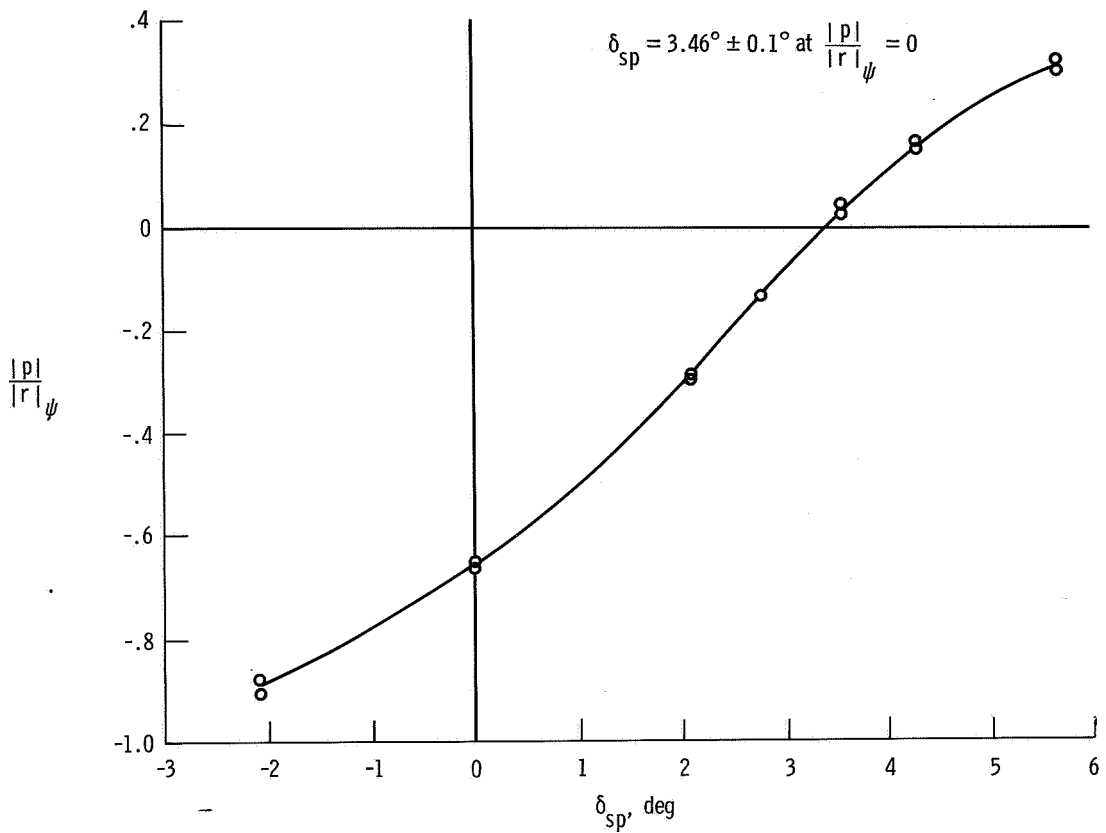
(a) Variation of $\dfrac{|p|}{|r|}_\psi$ with δ_{sp}.
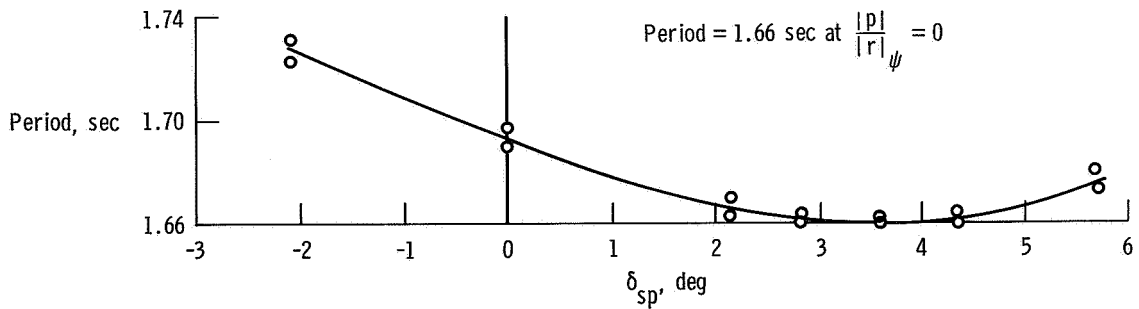
(b) Variation of period with δ_{sp}.

Figure 19. Determination of the inclination angle, δ_{sp}, of the spring plane and the period at which $\dfrac{|p|}{|r|}_\psi$ of the yaw mode is equal to zero in the single-point suspension test of the HL-10 lifting body vehicle.

54

The following tabulation of the experimentally determined and calculated inertial characteristics shows that in this instance a reasonably good correlation was obtained for all the characteristics except the inclination of the principal axis, and, consequently, the product of inertia. The vehicle weight was 23,344 newtons. For this test condition, the experimentally determined values are considered to be more accurate than the calculated values.

Quantity	Experimentally determined	Calculated
I_Z, kg-m^2	7441.0	7378.0
ε, deg	4.3	5.2
I_{XZ}, kg-m^2	443.0	534.0

CONCLUDING REMARKS

Current methods of experimentally determining aircraft center of gravity, moments of inertia, and product of inertia were reviewed.

For pitching- and rolling-moment-of-inertia determination, with the airplane mounted on and pivoted about knife edges, spring configurations can be set up that eliminate nonlinear spring moments at large amplitudes of oscillation.

Accurate values for the yawing moment of inertia, the product of inertia, and the inclination of the principal axis can be obtained from yaw-mode oscillation data acquired from tests that use a single-point suspension double-pendulum technique provided that the sway-mode effects are minimized by proper design of the suspension rig. Rocking-mode effects in the data can be isolated. The single-point suspension setup also provides an accurate determination of the location of the vertical center of gravity.

Care in conducting the experiment is essential. The springs must be calibrated accurately and pretensioned to avoid the nonlinear region of deflection at minimum loading conditions during perturbations. Precautions must be taken to prevent the introduction of undesirable secondary spring effects due to the cables or to structural deformations. In addition, the springs must be preloaded sufficiently to avoid any significant sag in the line of action of the springs. Precautions must also be taken to insure a minimum of extraneous damping of oscillatory motion.

Flight Research Center
National Aeronautics and Space Administration
Edwards, Calif., September 4, 1974

APPENDIX A

DETERMINATION OF THE CENTER OF GRAVITY OF THE HL-10 LIFTING BODY VEHICLE USING THE SINGLE-POINT SUSPENSION METHOD

The experimental setup for determining the center of gravity of the HL-10 lifting body vehicle by using the single-point suspension method illustrated by figure 3(a) is the same as the setup used to obtain the yawing moment of inertia and the product of inertia (figs. 10(b) and 18), except that springs are not used and the vehicle is tilted in pitch by the use of loading weights. Lead shot ballast was placed on the right outrigger (which was used for the spring attachment in the yaw tests) as shown in figure 18 to level the vehicle longitudinally and laterally to within ±0.08°. Tape measures were fastened to the vehicle at the reference rivet points (fig. 3(a)) normal to the horizontal reference axis and used in conjunction with a transit to obtain the tilt angle in pitch due to the loading weights.

The following tables summarize the detailed calculations made to obtain (1) the vertical center-of-gravity position of the vehicle with experimental equipment included and (2) the vertical and horizontal center-of-gravity positions with the experimental equipment removed. The loading coordinates x'_w and z'_w and the distance between the rivets, ℓ_r, are listed in figure 3(a).

TABLE A1.— VERTICAL CENTER-OF-GRAVITY POSITION OF EXPERIMENTAL CONFIGURATION

[Nose loading]

①	②			③			④		
Loading weight, w, N	Front tape, m			Rear tape, m			Change in average tape reading relative to zero loading		
	Increasing w	Decreasing w	Average	Increasing w	Decreasing w	Average	Front	Rear	Net
0	0.002	0.008	0.0050	0.118	0.121	0.1185	------	------	------
430.36	0.113	0.122	0.1175	0.156	0.159	0.1575	0.1125	0.0390	0.1515
652.77	0.173	0.178	0.1755	0.171	0.176	0.1735	0.1705	0.0550	0.2255
875.18	0.225	0.232	0.2285	0.194	0.195	0.1945	0.2235	0.0760	0.2995
1097.59	0.283	0.290	0.2865	0.210	0.213	0.2115	0.2815	0.0930	0.3745
1320.00	0.341	0.341	0.3410	0.227	0.227	0.2270	0.3360	0.1085	0.4445

①	⑤	⑥	⑦	⑧ (a)
Loading weight, w, N	$\tan\theta = \dfrac{Net}{\ell_r} = \dfrac{④}{2.964}$	$\dfrac{x'_w}{\tan\theta} = \dfrac{3.110}{⑤}$	$\dfrac{x'_w}{\tan\theta} - z'_w = ⑥ - 1.337$	$\bar{z}'_{ts} = \dfrac{w}{W_{ts}}\,⑦ = \dfrac{① \times ⑦}{24,309}$, m
0	------	------	------	-----
430.36	0.0511	60.861	59.524	1.054
652.77	0.0761	40.867	39.530	1.062
875.18	0.1010	30.792	29.455	1.060
1097.59	0.1263	24.264	23.287	1.051
1320.00	0.1500	20.733	19.396	1.054
				Average $\bar{z}'_{ts} = 1.056$

[a]Results in this column are plotted in figure 3(b).

TABLE A2.— VERTICAL CENTER-OF-GRAVITY POSITION OF CLEAN VEHICLE

①	②	③	④
Item	W, N (a)	Vertical distance from suspension bolt to center of gravity of item, m	Moment = ② × ③, N-m
Aircraft with test components	24,309.00	[b]1.056	25,670.304
Suspension beam	-733.95	[a]0.162	-118.900
Lead shot ballast	-142.34	[a]1.892	-269.307
Two outriggers	-88.96	[a]1.892	-168.312
	$W_{a/c} = \sum W = 23,343.75$		$\sum$ moments = 25,113.785

[a]From figure 3(a).
[b]From table A1.

The vertical position of the center of gravity of the clean vehicle below the suspension bolt pivot may be found as follows:

$$\bar{z}' = \frac{\sum \text{moments}}{\sum W} = 1.076 \text{ meters} \tag{A1}$$

The shift in vertical position of the center of gravity due to the removal of the experimental gear is defined as

$$\Delta \bar{z} = \bar{z}' - \bar{z}'_{ts} = 0.20 \text{ meter} \tag{A2}$$

The vertical position of the center of gravity below the horizontal reference identified by reference rivets (fig. 3(a)) can be determined as follows:

$$\bar{z}_r = \bar{z}' - z'_r = 1.076 - 0.884 = 0.192 \text{ meter} \tag{A3}$$

TABLE A3.— HORIZONTAL CENTER-OF-GRAVITY POSITION OF CLEAN VEHICLE

①	②	③	④
Item	W, N (a)	Horizontal distance from suspension axis to the center of gravity of item, m (a)	Moment = ② × ③, N-m
Aircraft with test components	24,309.00	0	0
Suspension beam	-733.95	-0.419	307.525
Lead shot ballast	-142.34	-0.089	12.668
Two outriggers	-88.96	-0.051	4.537
	$W_{a/c} = \sum W = 23,343.75$		$\sum$ moments = 324.730

[a]From figure 3(a).

The shift in the horizontal position of the center of gravity due to the removal of experimental gear can be determined from the following equation:

$$\Delta \bar{x} = \frac{\sum \text{moments}}{\sum W} = 0.014 \text{ meter forward of suspension line} \qquad \text{(A4)}$$

The fuselage station of the center of gravity of the clean vehicle can be found as follows:

$$\text{Fuselage station} = \text{Reference fuselage station} + x'_{\text{ref}} - \Delta \bar{x}$$

$$= \underbrace{3.632 - 0.359}_{\text{From figure 3(a)}} - 0.014 = 3.259 \text{ meters}$$

APPENDIX B

DETERMINATION OF THE YAWING MOMENT OF INERTIA, PRODUCT OF INERTIA, AND INCLINATION OF THE PRINCIPAL AXIS OF THE HL-10 LIFTING BODY VEHICLE USING THE SINGLE-POINT SUSPENSION DOUBLE-PENDULUM METHOD

Figures 10(b) and 18 show the test setup of the HL-10 lifting body vehicle for the determination of the yawing moment of inertia, product of inertia, and inclination of the principal axis. Figure 17 shows the locations of the centers of gravity of the test-setup components, and the location of the vehicle center of gravity (as obtained from appendix A) in the test-setup and clean configurations. In addition, figure 17 lists the linear spring constants of each of the four springs used in the setup.

The yaw-mode variation of the roll-to-yaw ratio and the period with the inclination of the spring plane, as obtained from test data, is summarized in figure 19. The only values of inclination angle of the spring plane and period of interest are those at which $\left.\dfrac{|p|}{|r|}\right|_\psi = 0$.

YAWING MOMENT OF INERTIA ABOUT THE VERTICAL REFERENCE AXIS THROUGH THE CENTER OF GRAVITY

Yawing Moment of Inertia, Including Test-Setup Components, About the Suspension Axis

The yawing moment of inertia for the test setup is obtained from

$$\left(I_{Z_s}\right)_{ts} = \frac{k_t \cos^2 \left(\delta_{sp}\right)_0}{\left(\omega_\psi\right)^2} = \frac{P^2 k_t \cos^2 \left(\delta_{sp}\right)_0}{4\pi^2} \tag{B1}$$

where, from figure 19 for $\left.\dfrac{|p|}{|r|}\right|_\psi = 0$,

$$\left(\delta_{sp}\right)_0 = 3.46°$$

and

$$P = 1.66 \text{ sec}$$

and, from figure 17,

$$k_t = \left(\ell_3'\right)^2 \left(k_1 + k_2 + k_3 + k_4\right)$$

$$= (1.935)^2 \ (7442 + 7413 + 7413 + 7544) \tag{B2}$$

$$= 111,626 \ \text{N-m/rad}$$

Thus,

$$\left(I_{Z_s}\right)_{ts} = 7784.00 \ \text{kg-m}^2$$

Yawing Moment of Inertia About Suspension Axis With Test-Setup Components Removed and Added Air Mass Effects Accounted For

The yawing moment of inertia of the clean vehicle about the suspension axis is obtained from the following equation:

$$I_{\underline{Z}_s} = \left(I_{Z_s}\right)_{ts} - \sum\left[I_{Z_0} + m\left(x_s^2 + y_s^2\right)\right]_{ec} - \Delta\left(I_{Z_s}\right)_{am} \tag{B3}$$

where

$$\left(I_{Z_s}\right)_{ts} = 7784.00 \ \text{kg-m}^2$$

$$\sum\left[I_{Z_0} + m\left(x_s^2 + y_s^2\right)\right]_{ec} = 127.40 \ \text{kg (obtained from the following table):}$$

①	②	③	④	⑤ Center of gravity (a)		⑥	⑦
Test-setup component	W, N	$m, \dfrac{②}{9.807},$ kg	I_{Z_0}, kg-m^2	x_s, m	y_s, m	$x_s^2 + y_s^2,$ m^2	$I_{Z_0} + m\left(x_s^2 + y_s^2\right)_{ec} = ④ + ③ \times ⑥,$ kg-m^2
Suspension beam	733.95	74.84	$\frac{1}{12} m_b l_b^2 = 46.82$	-0.419	0	0.176	60.00
Ballast	142.34	14.51	Negligible	-0.089	1.727	2.990	43.38
Left outrigger	44.48	4.54	Negligible	-0.051	-1.626	2.646	12.01
Right outrigger	44.48	4.54	Negligible	-0.051	1.626	2.646	12.01
							$\sum\left[I_{Z_0} + m\left(x_s^2 + y_s^2\right)\right]_{ec} = 127.40$ kg

[a]From figure 17.

The added air mass effect on I_{Z_s}, $\Delta\left(I_{Z_s}\right)_{am}$, was accounted for by using the procedure in reference 11. This was calculated to be 215.57 kg-m^2.

Thus,

$$I_{Z_s} = 7784.00 - 127.40 - 215.57 = 7441.03 \text{ kg-m}^2$$

Yawing Moment of Inertia of the Clean Vehicle About Its Z-Axis

The yawing moment of inertia of the clean vehicle about its Z-axis is obtained as follows:

$$I_Z = I_{Z_s} - \frac{W_{a/c}}{g}\left(\Delta\bar{x}\right)^2 \tag{B4}$$

where, from appendix A, $W_{a/c} = 23,343.75$ newtons and $\Delta\bar{x} = 0.014$ meter. Thus,

$$I_Z = 7441.03 - \frac{23,343.75}{9.807}(0.014)^2 = 7441.03 - 0.47$$
$$\approx 7441 \text{ kg-m}^2$$

PRODUCT OF INERTIA RELATIVE TO THE REFERENCE XZ-AXES THROUGH THE CENTER OF GRAVITY

Product of Inertia, With Test-Setup Components Included, About the $X_s Z_s$-Axes Passing Through the Suspension Line

The product of inertia for the test setup can be obtained as follows:

$$\left(I_{X_s Z_s}\right)_{ts} = \left(I_{Z_s}\right)_{ts} \tan\delta_{sp} \tag{B5}$$

where, from equations (B1) and (B2), $\left(I_{Z_s}\right)_{ts} = 7784.00$ kg-m^2 and, from figure 19, for $\left.\frac{|p|}{|r|}\right|_{\psi} = 0$, $\delta_{sp} = 3.46°$.

Thus, $\left(I_{X_s Z_s}\right)_{ts} = 470.64$ kg-m^2

Product of Inertia About $X_s Z_s$-Axes With Test-Setup Components Removed

The product of inertia of the clean vehicle about the $X_s Z_s$-axes is obtained from the following equation:

$$I_{X_s Z_s} = \left(I_{X_s Z_s}\right)_{ts} - \sum \left(I_{X_0 Z_0} + m x_s z_s\right)_{ec} \tag{B6}$$

where

$$\left(I_{X_s Z_s}\right)_{ts} = 470.64 \text{ kg-m}^2$$

$$\sum \left(I_{X_0 Z_0} + m x_s z_s\right)_{ec} = 26.60 \text{ kg-m}^2 \text{ (obtained from the following table):}$$

①	②	③	④	⑤		⑥	⑦
Test-setup component	W, N	m, $\frac{②}{9.807}$, kg	$I_{X_0 Z_0}$, kg-m²	Center of gravity (a)		$x_s z_s$, m²	$\left(I_{X_0 Z_0} + m x_s z_s\right)_{ec} = ④ + ③ \times ⑥,$ kg-m²
				x_s, m	z_s, m		
Suspension beam	733.95	74.84	Negligible	-0.419	-0.894	0.3750	28.06
Ballast	142.34	14.51	Negligible	-0.089	0.836	-0.0744	-1.08
Left outrigger	44.48	4.54	Negligible	-0.051	0.836	-0.0426	-0.19
Right outrigger	44.48	4.54	Negligible	-0.051	0.836	-0.0426	-0.19
							$\sum \left(I_{X_0 Z_0} + m x_s z_s\right)_{ec} = 26.60$ kg-m²

[a]From figure 17.

Thus,

$$I_{X_s Z_s} = 470.64 - 26.60 = 444.04 \text{ kg-m}^2$$

Product of Inertia of the Clean Vehicle About Its XZ-Axes

The product of inertia of the clean vehicle about its XZ-axes is obtained as follows:

$$I_{XZ} = I_{X_s Z_s} - \frac{W_{a/c}}{g} \left(\Delta \bar{x}\right)\left(\Delta \bar{z}\right) \tag{B7}$$

where, from table A2,

$$W_{a/c} = 23,343.75 \text{ newtons}$$

$$\Delta \bar{z} = 0.020 \text{ meter}$$

and, from table A3,

$$\Delta \bar{x} = 0.014 \text{ meter}$$

Thus,

$$I_{XZ} = 444.04 - \frac{23,343.75}{9.807}(0.014)(0.020) = 443.4 \text{ kg-m}^2$$

INCLINATION OF THE PRINCIPAL AXIS

With I_Z and I_{XZ}, as obtained in this appendix, equal to 7441.0 kg-m^2 and 443.4 kg-m^2, respectively, and I_X, as obtained from other sources, equal to 1625.0 kg-m^2, the inclination of the principal axis can be obtained by using equation (25):

$$\tan 2\varepsilon = \frac{2I_{XZ}}{I_Z - I_X} = 0.1525$$

from which

$$\varepsilon = 4.34° \text{ (below the reference X-axis)}$$

REFERENCES

1. Green, M. W.: Measurement of the Moments of Inertia of Full Scale Airplanes. NACA TN 265, 1927.

2. Miller, M. P.: An Accurate Method of Measuring the Moments of Inertia of Airplanes. NACA TN 351, 1930.

3. Soulé, Hartley A.; and Miller, Marvel P.: The Experimental Determination of the Moments of Inertia of Airplanes. NACA Rep. 467, 1933.

4. Gracey, William: The Experimental Determination of the Moments of Inertia of Airplanes by a Simplified Compound-Pendulum Method. NACA TN 1629, 1948.

5. Turner, Howard L.: Measurement of the Moments of Inertia of an Airplane by a Simplified Method. NACA TN 2201, 1950.

6. Notess, Charles B.; and Woodard, Claude R.: An Investigation of the Experimental Determination of Aircraft Inertia Characteristics. Tech. Rep. 53-207, Wright Air Dev. Center, 1953.

7. Boucher, Robert W.; Rich, Drexel A.; Crane, Harold L.; and Matheny, Cloyce E.: A Method for Measuring the Product of Inertia and the Inclination of the Principal Longitudinal Axis of Inertia of an Airplane. NACA TN 3084, 1954.

8. Woodfield, A. A.: Measurement of the Yawing Moment and Product of Inertia of an Aircraft by the Single Point Suspension Method: Theory and Rig Design. TR 68044, British R.A.E., 1968.

9. Mechtly, E. A.: The International System of Units – Physical Constants and Conversion Factors. Second Revision. NASA SP-7012, 1973.

10. Barnes, C. S.; and Woodfield, A. A.: Measurement of the Moments and Product of Inertia of the Fairey Delta 2 Aircraft. R & M No. 3620, British A.R.C., 1970.

11. Malvestuto, Frank S., Jr.; and Gale, Lawrence J.: Formulas for Additional Mass Corrections to the Moments of Inertia of Airplanes. NACA TN 1187, 1947.

"The aeronautical and space activities of the United States shall be conducted so as to contribute . . . to the expansion of human knowledge of phenomena in the atmosphere and space. The Administration shall provide for the widest practicable and appropriate dissemination of information concerning its activities and the results thereof."

—NATIONAL AERONAUTICS AND SPACE ACT OF 1958

NASA SCIENTIFIC AND TECHNICAL PUBLICATIONS

TECHNICAL REPORTS: Scientific and technical information considered important, complete, and a lasting contribution to existing knowledge.

TECHNICAL NOTES: Information less broad in scope but nevertheless of importance as a contribution to existing knowledge.

TECHNICAL MEMORANDUMS: Information receiving limited distribution because of preliminary data, security classification, or other reasons. Also includes conference proceedings with either limited or unlimited distribution.

CONTRACTOR REPORTS: Scientific and technical information generated under a NASA contract or grant and considered an important contribution to existing knowledge.

TECHNICAL TRANSLATIONS: Information published in a foreign language considered to merit NASA distribution in English.

SPECIAL PUBLICATIONS: Information derived from or of value to NASA activities. Publications include final reports of major projects, monographs, data compilations, handbooks, sourcebooks, and special bibliographies.

TECHNOLOGY UTILIZATION PUBLICATIONS: Information on technology used by NASA that may be of particular interest in commercial and other non-aerospace applications. Publications include Tech Briefs, Technology Utilization Reports and Technology Surveys.

Details on the availability of these publications may be obtained from:

SCIENTIFIC AND TECHNICAL INFORMATION OFFICE

NATIONAL AERONAUTICS AND SPACE ADMINISTRATION

Washington, D.C. 20546